AGU PUBLICATIONS

JGR

Journal of Geophysical Research: Earth Surface

RESEARCH ARTICLE
10.1002/2016JF003915

Key Points:
- Backwater-mediated deltas grow through cycles of lobe deposition and avulsion
- We quantify avulsion trigger, flow path selection, channel abandonment, and depositional signatures
- Bed thickness recorded in strata reflects the morphologic measurements of avulsion setup process

Supporting Information:
- Supporting Information S1
- Movie S1
- Movie S2

Correspondence to:
V. Ganti,
v.ganti@imperial.ac.uk

Citation:
Ganti, V., A. J. Chadwick, H. J. Hassenruck-Gudipati, and M. P. Lamb (2016), Avulsion cycles and their stratigraphic signature on an experimental backwater-controlled delta, *J. Geophys. Res. Earth Surf.*, *121*, doi:10.1002/2016JF003915.

Received 11 APR 2016
Accepted 15 AUG 2016
Accepted article online 17 AUG 2016

Avulsion cycles and their stratigraphic signature on an experimental backwater-controlled delta

Vamsi Ganti[1,2], Austin J. Chadwick[1], Hima J. Hassenruck-Gudipati[1,3], and Michael P. Lamb[1]

[1]Division of Geological and Planetary Sciences, California Institute of Technology, Pasadena, California, USA, [2]Department of Earth Science and Engineering, Imperial College London, London, UK, [3]Now at Department of Geological Sciences, Jackson School of Geosciences, University of Texas at Austin, Austin, Texas, USA

Abstract River deltas grow in large part through repeated cycles of lobe construction and channel avulsion. Understanding avulsion cycles is important for coastal restoration and ecology, land management, and flood hazard mitigation. Emerging theories suggest that river avulsions on lowland deltas are controlled by backwater hydrodynamics; however, our knowledge of backwater-controlled avulsion cycles is limited. Here we present results from an experimental delta that evolved under persistent backwater hydrodynamics achieved through variable flood discharges, shallow bed slopes, and subcritical flows. The experimental avulsion cycles consisted of an initial phase of avulsion setup, an avulsion trigger, selection of a new flow path, and abandonment of the parent channel. Avulsions were triggered during the largest floods (78% of avulsions) after the channel was filled by a fraction (0.3 ± 0.13) of its characteristic flow depth at the avulsion site, which occurred in the upstream part of the backwater zone. The new flow path following avulsion was consistently one of the shortest paths to the shoreline, and channel abandonment occurred through temporal decline in water flow and sediment delivery to the parent channel. Experimental synthetic stratigraphy indicates that bed thicknesses were maximum at the avulsion sites, consistent with our morphologic measurements of avulsion setup and the idea that there is a record of avulsion locations and thresholds in sedimentary rocks. Finally, we discuss the implications of our findings within the context of sustainable management of deltas, their stratigraphic record, and predicting avulsions on deltas.

1. Introduction

River deltas are of immense socioeconomic importance because they host over half billion people worldwide [*Syvitski et al.,* 2009; *Vörösmarty et al.,* 2009] and are currently under threat of drowning and destruction due to relative sea level rise, anthropogenic interference, and oceanic storms [*Meybeck and Vörösmarty*, 2005; *Syvitski and Saito*, 2007; *Blum and Roberts*, 2009; *Syvitski et al.,* 2009; *Vörösmarty et al.,* 2009; *Tessler et al.,* 2015]. Many river deltas derive their fan-shaped planform morphology through river avulsions, which are characterized by abrupt "channel jumping" as opposed to gradual channel migration [*Allen*, 1965; *Slingerland and Smith*, 2004]. River avulsions set the fundamental length scale of deltas and are the primary means by which sediment and water are distributed across the deltaic plain [e.g., *Jerolmack*, 2009]. Moreover, river avulsions present a serious hazard to communities living on deltas worldwide, and understanding their mechanics is vital for sustainable management of deltas, and forecasting deltaic evolution in the face of sea level rise, river engineering, and land use changes upstream of river deltas. From a stratigraphic viewpoint, river avulsions control the distribution of sediment and the stacking patterns of channel bodies in the subsurface [e.g., *Allen*, 1979; *Bridge and Mackey*, 1993; *Mackey and Bridge*, 1995; *Mohrig et al.,* 2000; *Hajek et al.,* 2012], and thus are of significant importance for unraveling the mechanics of ancient deltaic systems [e.g., *Paola*, 2000; *Kleinhans*, 2005; *Bianchi and Allison*, 2009; *DiBiase et al.,* 2013], and for characterization of aquifers and hydrocarbon reservoirs [*Bohacs and Suter*, 1997; *Ainsworth et al.,* 1999].

River avulsions occur repeatedly on deltas, and the depositional sequence that leads to an avulsion and the subsequent abandonment of a channel is often referred to as an "avulsion cycle" [e.g., *Hoyal and Sheets*, 2009; *Reitz and Jerolmack*, 2012]. Figure 1 shows a schematic summary of previous ideas on the avulsion cycle, which can be characterized by four main stages: setup, trigger, path selection, and abandonment. Mouth bar deposition is thought to force an upstream wave of in-channel deposition (Figure 1a) [*Edmonds et al.,* 2009; *Hoyal and Sheets*, 2009; *Reitz and Jerolmack*, 2012], render the channel unstable and poised for an avulsion; the antecedent processes leading up to this inherently unstable configuration are often referred to as the avulsion "setup" [e.g., *Jones and Schumm*, 1999; *Mohrig et al.,* 2000; *Slingerland and Smith*, 2004].

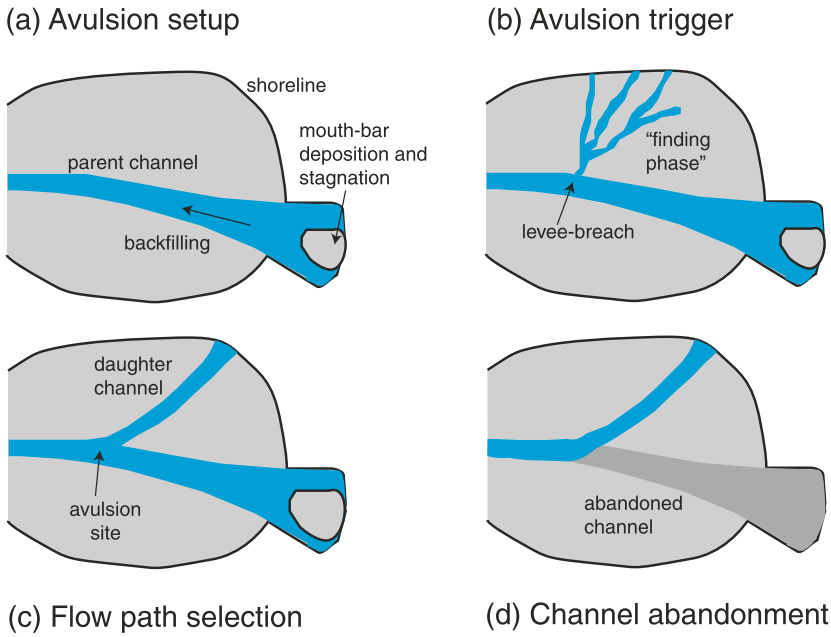

Figure 1. Schematic summary of the processes that describe an avulsion cycle. (a) Channelization of the flow leads to the formation of the parent channel, which results in deposition at the river mouth, mouth bar formation, and delta progradation. In time, the river mouth bar stagnates and results in an upstream migrating wave of deposition and in-channel backfilling. (b) Channel bed aggradation leads to increased likelihood of overbank flooding upstream, which results in an (c) avulsion and relocation of the channel into a new flow path. (d) Flow path selection of the daughter channel is accompanied by partial or complete abandonment of the parent channel. Gray and blue colors indicate land and water, respectively.

Although river avulsion is a stochastic process [e.g., *Mohrig et al.,* 2000; *Jerolmack and Mohrig*, 2007; *Jerolmack and Paola*, 2007], the critical amount of aggradation, h^*, required to initiate an avulsion is on average thought to be proportional to the channel depth

$$h^* = {}^{h_{\mathrm{fill}}}\!/_{h_c} \tag{1}$$

where h_c is the bankfull channel depth at the avulsion site and $h_{\mathrm{fill}} = v_A T_{\mathrm{ma}}$ is the amount of vertical aggradation, occurring at rate v_A, that accumulates within a measured avulsion timescale, T_{ma}(Figure 2) [*Bryant et al.,* 1995; *Jerolmack and Mohrig*, 2007; *Jerolmack*, 2009; *Reitz and Jerolmack*, 2012]. Some have argued that the appropriate length scale in equation (1) is the superelevation height of the levees above the surrounding floodplain [*Mackey and Bridge*, 1995; *Heller and Paola*, 1996; *Mohrig et al.,* 2000; *Hajek and Wolinsky*, 2012]. The relation given by equation (1) has also been inferred from ancient preserved channel and levee deposits that record the postavulsion configurations of the parent channel [e.g., *Mohrig et al.,* 2000; *Hajek and Wolinsky*, 2012].

Following the setup phase, channel bed aggradation results in an increased likelihood of overbank flows, and the avulsion "trigger" is thought to be a short timescale event, which causes the water flow to leave the channel (e.g., overbank flooding), which may occur via a levee breach (Figure 1b) [*Mohrig et al.,* 2000; *Slingerland and Smith*, 2004; *Edmonds et al.,* 2009; *Hajek et al.,* 2012], and result in a river avulsion. As overbank flow occurs, several incipient channels may develop on the floodplain—referred to as the "finding phase" (Figure 1b) [*Hoyal and Sheets*, 2009; *Martin et al.,* 2009; *Reitz and Jerolmack*, 2012]—before the selection of the new (daughter) channel path (Figure 1c). Previous numerical [*Jerolmack and Paola*, 2007], experimental [*Reitz et al.,* 2010], field [e.g., *Jain and Sinha*, 2003], and stratigraphic observations [e.g., *Aslan et al.,* 2005] suggest that channels often reoccupy their former paths from previous avulsion cycles. The last phase of an avulsion cycle is the abandonment of the parent channel where all the incoming water discharge is eventually captured by the daughter channel (Figure 1d). Abandoned channels may be filled through overbank deposition [e.g., *Mohrig et al.,* 2000] and through tie channel deposition [e.g., *Rowland et al.,* 2005].

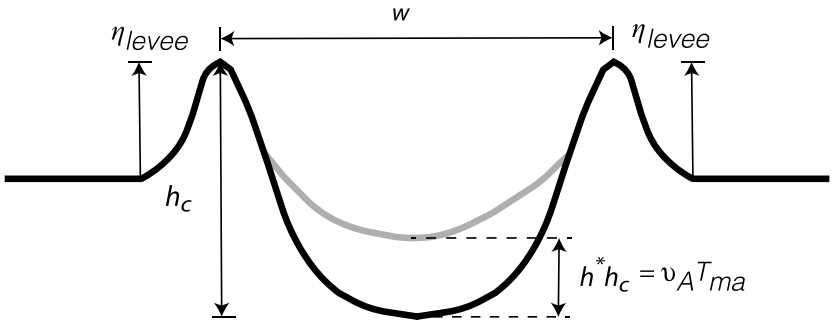

Figure 2. Definition sketch of a channel cross section at the avulsion site highlighting the top width of the channel (w), characteristic flow depth (h_c), and the levee elevation measured above the sea level (η_{levee}). The avulsion setup arises from in-channel sedimentation by a critical amount of the characteristic flow depth (h^*h_c), which scales with the net aggradation rate and the avulsion timescale ($\upsilon_A T_{\text{ma}}$; equation (1)).

Avulsions may be accompanied by partial abandonment of the parent channel such that multiple channels persist over time [e.g., *Slingerland and Smith*, 2004].

Most descriptions of the avulsion cycle do not explicitly incorporate backwater hydrodynamics; however, there are reasons to expect that the avulsion cycle is strongly influenced by backwater. The backwater zone is a region of nonuniform flow, forced by a stable sea level at the river mouth, that produces spatial deceleration and deposition during low flows, and spatial acceleration and erosion during high flows [e.g., *Chow*, 1959; *Chatanantavet et al.,* 2012; *Lamb et al.,* 2012; *Nittrouer et al.,* 2012; *Chatanantavet and Lamb*, 2014]. While often not the case for laboratory-scale deltas, most natural river deltas of large lowland rivers have sufficiently low bed slopes and subcritical Froude numbers ($Fr < 1$) such that backwater effects dominate the hydrodynamics and sediment transport in near the coast [e.g., *Bresse*, 1860; *Chow*, 1959; *Lamb et al.,* 2012; *Nittrouer et al.,* 2012]. The scale parameter that determines the length scale over which these nonuniform flows prevail is known as the backwater length, L_b, which can be approximated as the ratio of the characteristic flow depth and the channel bed slope [e.g., *Paola*, 2000], although channel geometry, Froude number, and flood stage height also affect the length of the backwater zone [*Lamb et al.,* 2012].

Although deltaic evolution is influenced by a wide variety of natural processes such as waves, tides, vegetation, sediment cohesion, and buoyancy gradients, field observations suggest that the avulsion length and consequently the lobe size of many deltas, L_A, tend to scale to first order with the backwater length with the ratio of the avulsion length to backwater length ranging from about 0.5 to 1 [*Jerolmack and Swenson*, 2007; *Jerolmack*, 2009; *Chatanantavet et al.*, 2012; *Ganti et al.*, 2014, 2016], implying that backwater hydrodynamics strongly affects the setup or trigger or both for lobe-scale avulsions. This idea is supported by numerical modeling of *Chatanantavet et al.* [2012] and recent experiments [*Ganti et al.,* 2016] which showed that the variable floods in a backwater-controlled coastal river can produce a locus of in-channel deposition, and therefore a location of enhanced setup, that scales with the backwater length. Further, through analysis of a number of natural deltas, *Ganti et al.* [2014] showed that threshold depth of channel sedimentation needed to induce an avulsion (h^*) may be reduced in backwater-dominated rivers with high flood variability. To our knowledge the path selection and abandonment processes have not been investigated in the context of backwater hydrodynamics, but an effect might be expected since backwater strongly influences water and sediment transport patterns in coastal rivers [*Lamb et al.,* 2012; *Nittrouer et al.,* 2012].

Because river avulsions on deltas occur over relatively long timescales of tens to thousands of years [e.g., *Jerolmack and Mohrig*, 2007], laboratory experiments have been an important tool to observe and analyze the avulsion cycle [*Edmonds et al.,* 2009; *Hoyal and Sheets*, 2009; *Martin et al.,* 2009; *van Dijk et al.,* 2009; *Reitz and Jerolmack*, 2012; *Hamilton et al.,* 2013]. Experiments are by definition simplified representations of the essential processes that govern the depositional dynamics at larger, field scales, and these experimental techniques rely on similarity arguments put forth by *Hooke* [1968] and *Paola et al.* [2009]. Although emerging theories suggest that persistent backwater hydrodynamics may play a key role in avulsion dynamics on deltas [*Chatanantavet et al.,* 2012; *Chatanantavet and Lamb*, 2014; *Ganti et al.,* 2016], these dynamics are often difficult to achieve at reduced scale owing to the low channel slopes necessary to make subcritical Froude

numbers, large facilities necessary to encompass the full backwater zone [e.g., *Hotchkiss and Parker*, 1991], and variable flood discharges necessary to make a persistent backwater zone [*Chatanantavet et al.,* 2012; *Chatanantavet and Lamb*, 2014; *Ganti et al.,* 2016]. Although *Chatanantavet and Lamb* [2014] produced persistent backwater effects in an experimental coastal river, their experimental channel depths were on the order of ~10 cm and the dimensions of the ocean basin were small such that they did not produce a delta composed of multiple lobes built through repeated avulsions.

Recently, *Ganti et al.* [2016] reported on physical experiments that capture delta growth in the presence of persistent backwater hydrodynamics, and they showed that their experimental delta grew through deposition of multiple lobes in which the lobe size at abandonment (L_A) scaled with the backwater length (L_b). Here we report on new results from the same experiment as *Ganti et al.* [2016] focusing on the avulsion cycle, which they did not address. In particular, we document the avulsion setup, trigger, path selection, and abandonment phases. Further, we present results pertaining to how the depositional processes of an avulsion cycle are recorded in the experimental stratigraphy. We begin with a review of the experiments and the experimental methods, followed by results and discussion.

2. Experimental Arrangement and Methods

2.1. Experimental Arrangement

The experiments presented here were first reported by *Ganti et al.* [2016], and here we summarize the essential details of their experimental arrangement and data collected. *Ganti et al.* [2016] presented a comparative study of avulsion locations on two experimental deltas, where in one experimental delta growth was controlled by persistent backwater hydrodynamics under variable flood discharges, while the other experimental delta grew under constant flow and sediment input conditions, and consequently backwater hydrodynamics were muted. Consistent with numerical modeling by *Chatanantavet et al.* [2012], *Ganti et al.* [2016] found that floods of differing discharge are needed to produce persistent backwater hydrodynamics; under constant discharge conditions sedimentation fills in overdeepened parts of the channel resulting in near normal-flow conditions everywhere. The experimental delta from *Ganti et al.* [2016] that had persistent backwater hydrodynamics grew through deposition of multiple lobes that maintained a constant size, which scaled with the backwater length [*Ganti et al.,* 2016], similar to scaling relations for natural lowland deltas [*Jerolmack and Swenson*, 2007; *Ganti et al.,* 2014]. Further, they found that the avulsion locations translated seaward in step with shoreline progradation, consistent with the hypothesis presented in *Ganti et al.* [2014]. This was in contrast to the experimental delta without persistent backwater hydrodynamics, where avulsion nodes were fixed at the tank boundary and the delta grew in time to fill the basin, analogous to alluvial fans and fan-deltas.

In this manuscript, we extract new data on the avulsion cycle from the experimental delta of *Ganti et al.* [2016] that used variable discharge flood events and persistent backwater hydrodynamics. We do not address the constant discharge delta. The experiments were conducted in the river-ocean facility at the Caltech Earth Surface Dynamics Laboratory, where a 7 cm wide, 7 m long alluvial river drained into a 5 m by 3 m "ocean" basin with 10 cm deep standing water (Figure 3). Sediment and water were fed at the upstream end of the alluvial river, and sea level was held constant during the experiments using a programmable stand pipe at the downstream end of the ocean basin. To achieve persistent backwater hydrodynamics that result from variable flood discharges, we oscillated between a 40 min low flow and 15 min high flow for 160 cycles (Table 1). The duration of each flow was scaled such that the deposition caused by the low flow was not balanced by the erosion caused by the high flow following the modeling of *Chatanantavet et al.* [2012], resulting in persistent backwater hydrodynamics that forced the experimental alluvial river to be in a state of perpetual morphodynamic disequilibrium within the backwater zone (see Materials and Methods in *Ganti et al.* [2016]).

The experiment was conducted under subcritical flow conditions (Table 1), which was achieved by using crushed walnut shells of uniform grain diameter ($D = 0.7$ mm; $\rho_s = 1300$ kg/m^3) as the sediment. During our experiments, sediment transport primarily occurred as bed load with some suspension during the high flow conditions. The choice of the experimental water and sediment discharges was guided by a quasi-2D, coupled hydrodynamic and morphodynamic model [*Chatanantavet et al.,* 2012; *Lamb et al.,* 2012; *Chatanantavet and Lamb*, 2014] such that both discharge events created an equivalent bed slope with measurable differences between flow depths under normal-flow conditions in which sediment transport

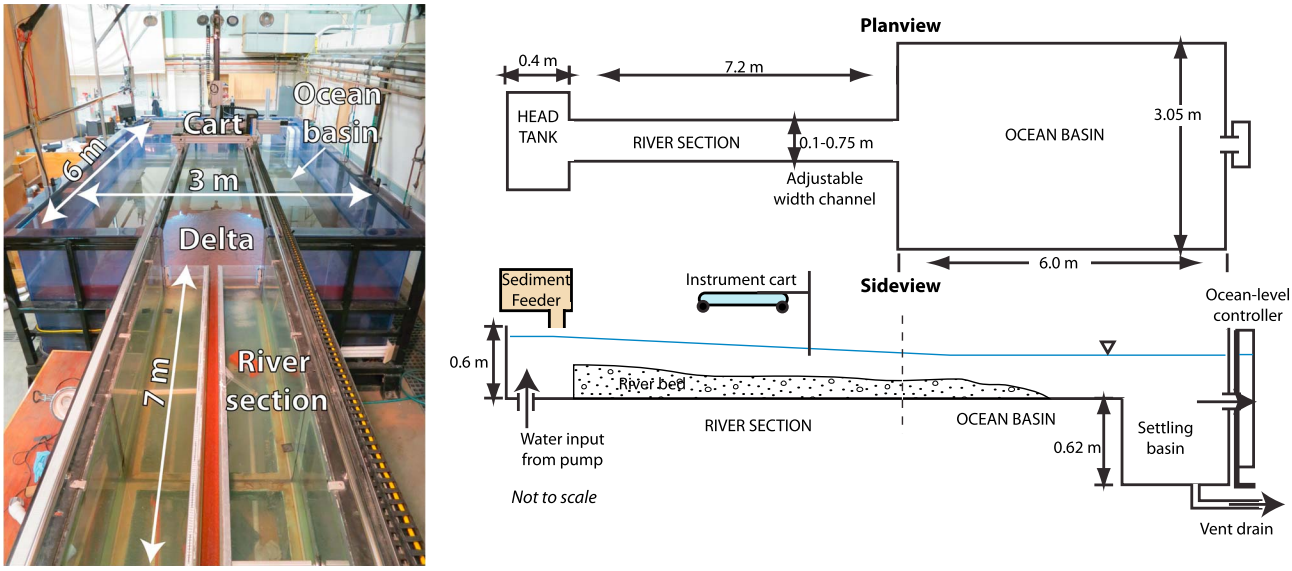

Figure 3. Annotated perspective image of the river-ocean facility in the Earth Surface Dynamics Laboratory at the California Institute of Technology, which highlights the alluvial river section, delta top, instrument cart, and the ocean basin. Also shown are the plan view and side view of the experimental facility. Note that while the ocean basin was 6 m long, we laid a false floor for the first 5 m of this section such that the water depth above the false floor was 10 cm. Figure reproduced from *Ganti et al.* [2016].

was at capacity, the river was in morphodynamic disequilibrium within the backwater zone, and computed backwater length was within the confines of the flume (Table 1; see Materials and Methods of *Ganti et al.* [2016] for additional details). Thus, erosion and deposition occurred in the experiment due to backwater effects alone and not because of imbalances in the input water and sediment fluxes. The river section of the flume was long enough (7 m) such that normal-flow conditions and a constant bed slope for both flood events could be validated upstream of the backwater zone (Table 1).

2.2. Experimental Data Collection

An ultrasound distance meter (Massa) and a laser triangulation sensor (Keyence) measured the water surface elevation during the experiment at 1 mm vertical resolution and the bed topography at 0.1 mm resolution

Table 1. Measured and Estimated Parameters Within the Normal Flow Reach of the Experimental River [*Ganti et al.*, 2016]

Quantity	Low Flow	High Flow
Water discharge, Q_w (l/min)	8.3	12.0
Sediment feed, Q_s (g/min)	36	60
Run time	40 min[a]	15 min[a]
Normal-flow depth[b], h_n (mm)	9.5	13.0
Normal Froude number[b], Fr (−)	0.67	0.63
Measured channel bed slope[b], S (−)	3.3×10^{-3}	3.3×10^{-3}
Shields number[c], τ_* (−)	0.15	0.20
Particle Reynolds number[d], Re_p (−)	39.71	
Critical Shields stress[e], τ_{*c} (−)	0.036	
Rouse number[f] (−)	4.5	3.8
Number of avulsions	9	32

[a]The low-flow and high-flow events were repeated for 160 times resulting in a total experimental runtime of ~150 h.
[b]Normal-flow depth, Froude number, and channel bed slope were estimated within the first 3 m of the experimental river and averaged over the experimental runtime (see Materials and Methods in *Ganti et al.* [2016] for additional details).
[c]Shields number was computed using $\tau_* = \tau_b/(\rho_s - \rho)gD$, where $\tau_b = \rho g h_n S$. Applying a sidewall correction using the empirical equation of *Williams* [1970] did not change this value by more than 1%.
[d]Particle Reynolds number was computed using the following relation: $Re_p = \sqrt{((\rho_s - \rho)/\rho)gD^3}/\upsilon$, where $\upsilon = 0.8 \times 10^{-6}$ m^2/s is the dynamic viscosity of water at 30°C.
[e]Critical Shields stress was computed using the calculated Re_p and the approximation of *Miller et al.* [1977].
[f]Rouse number was computed as the ratio of settling velocity of sediment (32 mm/s) to the product of the von Karman constant and the bed shear velocity [*Ganti et al.*, 2016].

when the flow was switched off, respectively. Both instruments collected data while mounted on a motorized 3-D positioning instrument cart with submillimeter horizontal accuracy. We collected water surface elevation at the beginning and end of each flow event (i.e., low and high flows). Water flow was switched off at the end of each flow event, and bed surface elevation data were collected for the whole delta at a horizontal resolution of 3 mm by 3 mm. The ocean basin was not drained at the end of each flow event, and the bed elevation measurements of the submerged part of the delta were empirically corrected for the refraction index of Keyence beam through still water. The combined error in vertical measurements from the instrument error and the empirical correction for the refraction index was ±0.1 mm. The raw data were denoised using a moving median filter of kernel-size 1.5 cm (see Materials and Methods in *Ganti et al.* [2016] for details of data filtering).

Six mounted cameras bordered the experimental facility (Figure 3), each simultaneously capturing overhead images of the deltaic evolution at a temporal resolution of 1 min for the whole duration of the experiments (supporting information Movie S1). These cameras were also used to capture videos (at a rate of 59 fps) of the transport of fluorescent dye pulses, which were introduced just upstream of the tank boundary (supporting information Movie S2). These dye videos were used for estimating the water surface velocity of both low and high flows through the backwater reach. The pixel coordinates of both the overhead images and videos were converted to instrument cart coordinates using multiple orthogonal tape measures on the ocean basin floor together with overhead images captured when the basin was dry (see Materials and Methods in *Ganti et al.* [2016] for details).

2.3. Data Analysis

We computed the in-channel deposition and erosion using the topographic scans taken at the end of each flow event. In the confined portion of the experimental alluvial river (Figure 3), we directly computed the difference between the bed topography at the end of a given flow event and the bed topography from the end of the preceding flow event to quantify the amount of deposition/erosion that occurred during the event. On the delta topset, we computed the channel bed elevation by extracting the cross-sectional topography perpendicular to the channel thalweg from the topographic scans taken at the end of each flow event. We used the overhead imagery of deltaic evolution and the dye videos during the flow events as a guide to identify the channel thalweg from the topographic scans. Once we extracted the cross-sectional topography along the channel thalweg, we measured the channel width (w) by computing the distance between the locations of the levees on either side of the channel thalweg (Figure 2). To account for the variability in channel widths and channel elevations, we computed the cross-section-averaged bed elevation (η_{bed}) as

$$\eta_{bed} = \eta_{levee} - \frac{A_{cs}}{w} \tag{2}$$

where η_{levee} is the mean of the levee elevation on either side of the channel thalweg (Figure 2), and A_{cs} is the computed cross-sectional area of the channel.

We used the overhead dye videos (frame rate of 59 fps) to compute the water surface velocity on the deltaic plain during both low- and high-flow events (supporting information Movie S2). The color contrast between the dye (fluorescent) and the deltaic surface (brown) was used to automatically identify the location of the dye in each frame of the video, which was converted into a binary matrix of "dye" and "no dye." We manually tracked the location of the dye front in each frame of the video and estimated the distance traveled by the dye along the channel thalweg in successive frames. This computed distance was converted into instantaneous surface velocity using central differencing. Finally, the instantaneous surface velocity data were smoothed using a moving window average filter of kernel-size 25 cm, which was approximately the channel width on the delta top during the later phase of delta growth. The computed water surface velocity is higher than the depth-averaged flow velocity as expected.

We identified both the avulsion locations and the shorelines on the concatenated images of deltaic evolution whose pixel coordinates were transformed into the coordinates of the instrument cart following calibration using the tape measures. We defined an avulsion as the development of a new channel whereby the daughter channel captured flow through consecutive flow events and the parent channel was partially or completely abandoned. The avulsion site was chosen to be the location where a levee breach was initiated,

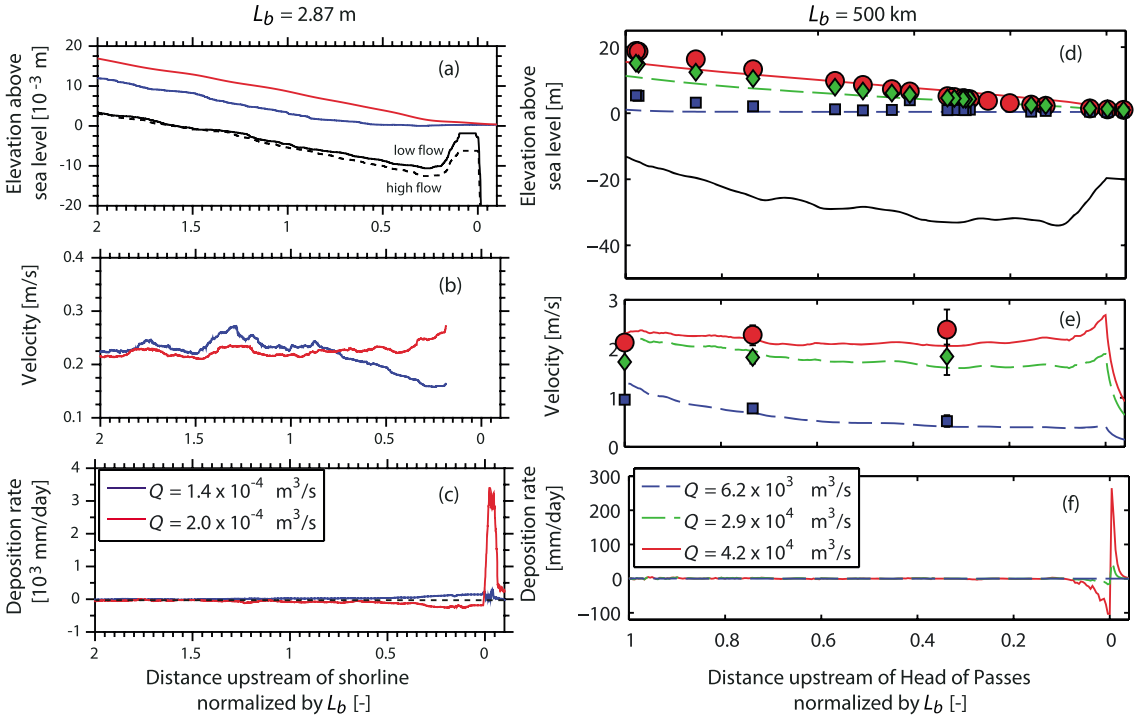

Figure 4. (a) Plot showing the bed and water surface profiles for consecutive low- and high-flow events early in the experiment (t = 4.75–5.7 h), which show the concave up and convex up nature of the water surface profiles during low- and high-flow events, respectively. (b) Cross-section-averaged flow velocity for both the flow events shows the flow deceleration and flow acceleration during low- and high-flow events, respectively. (c) The flow deceleration during low flow was accompanied by sediment deposition within the backwater reach, and the flow acceleration during high flow was accompanied by erosion. (d) Bed and water surface elevation, (e) depth-averaged flow velocity, and (f) computed deposition and erosion rates for the Mississippi River within its backwater zone (L_b = 500 km) are shown for comparison [*Lamb et al.,* 2012]. The three water discharges (Q) represent typical base flow (blue), 2 year (green), and 30 year (red) return-period flood events for the Lower Mississippi River, and the markers are field observations and the solid and dashed lines are model predictions of *Lamb et al.* [2012]. The backwater length was computed as the ratio of the low-flow normal-flow depth and the normal-flow bed slope for the experiment (L_b = 2.87 m).

and we did not observe significant migration of the avulsion site during the process of creation of the daughter channel [*Ganti et al.,* 2016]. While this manual identification procedure involved some inherent subjectivity, our results on avulsion length had an error that is significantly less than the backwater length and less than the channel width at the avulsion site [*Ganti et al.,* 2016]. Our definition of avulsion in the experiment precludes the characterization of crevasse splays as avulsion events. During high-flow events, crevasse splays resulted in overbank flooding and channelization on the floodplain; however, splays were not active during low-flow events.

We constructed the synthetic stratigraphy from the topographic scans collected at the end of each flow event. We identified erosional boundaries at each location of the delta as the lowest elevation in time such that no future elevation at that point was lower than this given value (see *Ganti et al.* [2011] and *Ganti et al.* [2013] for example applications of this method). The bulk porosity remained constant through the experiment within an error of ±10% indicating that compaction between scans and through the experiment was negligible. Although we did not physically take stratigraphic cuts at the end of our experiment due to the lack of grain size variation, previous workers have reported good agreement between physical stratigraphy and the synthetic stratigraphy constructed from elevation time series in an experimental, avulsion-dominated fan system [*Straub et al.,* 2012].

3. Results

3.1. Observations of Transient Backwater Hydrodynamics and a Proto-Delta

We first document the backwater and drawdown hydrodynamics observed in the experiment along with their effect on morphodynamics of the experimental alluvial river. Experimental data of water surface

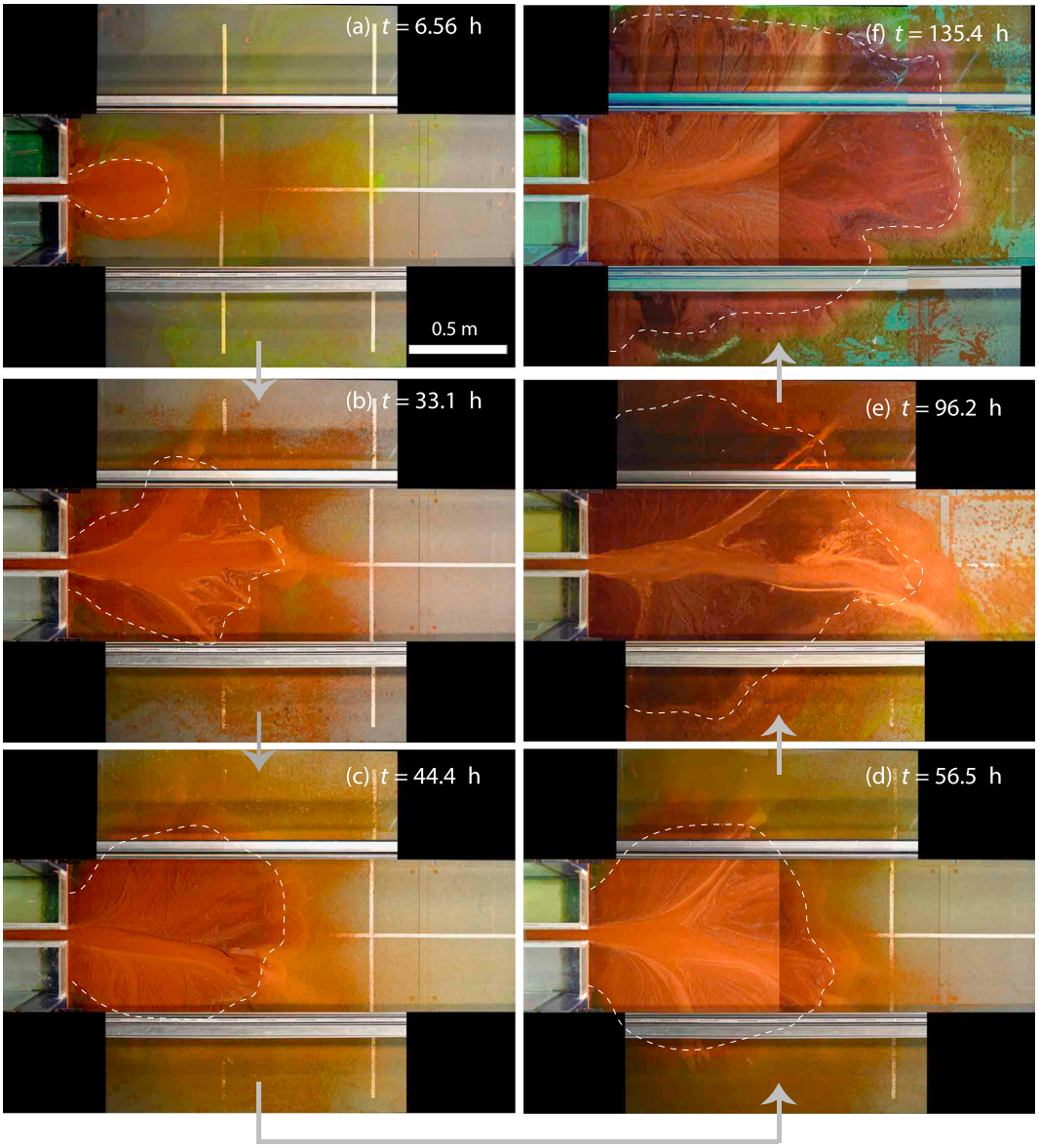

Figure 5. (a–f) Plate of pictures showing delta growth during the experiment. The scale for the pictures is shown in the lower right corner of Figure 5a, and the white dashed lines indicate the shorelines. The two silver horizontal bars are instrument rails that sit above the experiment.

elevation demonstrate that during low flow the water surface elevation was concave up with a small water surface slope (M1 curve [sensu *Chow*, 1959]; blue solid line in Figure 4a), and during high-flow event the water surface profile was convex up with steep water surface slope (M2 curve [sensu *Chow*, 1959]; red line in Figure 4a). The bed and water surface profiles within the backwater zone were not parallel to each other, and channel widths were relatively uniform, indicating that nonuniform flows prevailed within the backwater zone of the experimental alluvial river. We computed the cross-sectionally averaged flow velocity using the measurements of water stage height, bed elevation, and the water discharge (Figure 4b). Results show that low-flow events were characterized by spatially decelerating flows, which resulted in sediment deposition in the backwater zone of the experimental alluvial river (blue lines in Figures 4b and 4c). In contrast, the high-flow event was characterized by spatially accelerating flow and sediment erosion in the lowest portions of the experimental alluvial river (red lines in Figures 4b and 4c). The experimental data of water surface profiles, flow velocities, and the patterns of erosion and deposition within the backwater zone are consistent with numerical models and field

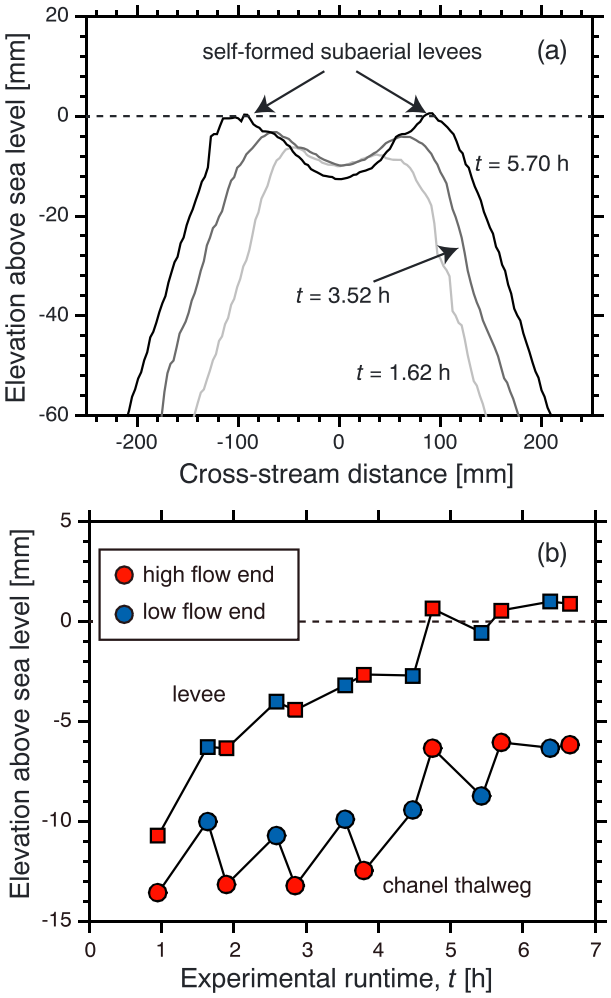

Figure 6. (a) Plot showing the temporal evolution of the cross-sectional topography of the delta lobe 10 cm downstream of the imposed change in confinement in the experimental facility. During the first 6 h of the experiment, the delta lobe grew radially with self-channelization occurring at approximately 5.7 h. (b) Temporal evolution of the channel thalweg, which was defined as the center of the flume, and the levee elevation that was computed as the maximum elevation along the flanks of the channel thalweg. The red and blue markers indicate bed and levee elevation at the end of high- and low-flow events, respectively. Self-channelization occurred in our experiment through repeated and alternating thalweg erosion during high flow, and deposition along the thalweg and at locations away from the longitudinal axis of the lobe.

observations of these quantities within the backwater zone of the Mississippi River (as shown in Figures 4d–4f [*Lamb et al.,* 2012]). These results indicate that the patterns of deposition and erosion resulting from flood variability within the backwater zone were similar across experimental and field deltas despite 5 orders of magnitude difference in the length scales (Figure 4). Figure 4 also highlights the transient nature of bed adjustment to variable flood discharges within the backwater zone, which resulted in persistent backwater hydrodynamics because neither flow was run for long enough to attain their respective equilibrium, normal-flow conditions. This is consistent with the experiments of *Chatanantavet and Lamb* [2014] but demonstrated here on a delta.

The experimental delta grew through regular avulsion cycles after an initial phase of sheet flow. Figure 5 shows a photographic overview of deltaic evolution in our experiment (see also supporting information Movie S1). Once the experiment started, the experimental alluvial river deposited sediment at the river mouth, and the depositional lobe grew in time through sheet flow on the lobe surface (Figure 5a and supporting information Movie S1). This resulted in a radially symmetric lobe with deeper flows down the centerline of the flume and shallow flows on portions of the lobe away from the flume centerline. The flow was channelized after approximately 5.7 h, which resulted in elongation of the lobe at the location of the river mouth. Self-channelization occurred through repeated and alternating thalweg erosion during high flow and deposition along the channel thalweg and flanks during low flow (Figure 6), similar to *Chatanantavet and Lamb* [2014]. The channelization of the flow was accompanied by transient mouth bar deposition and channel bifurcation at the tips of the main channel (supporting information Movie S1). At this point in our experiments, our results are qualitatively similar to those of *Chatanantavet and Lamb* [2014] in that we observed transient morphodynamic adjustment of the channel bed in response to flood events, a persistent backwater zone, and a single delta lobe offshore, cut by a self-made and leveed channel. *Chatanantavet and Lamb* [2014] did not run their experiments long enough (nor was facility large enough) to observe the avulsion-cycle dynamics and the construction and abandonment of multiple deltaic lobes. This is our focus in the rest of the paper.

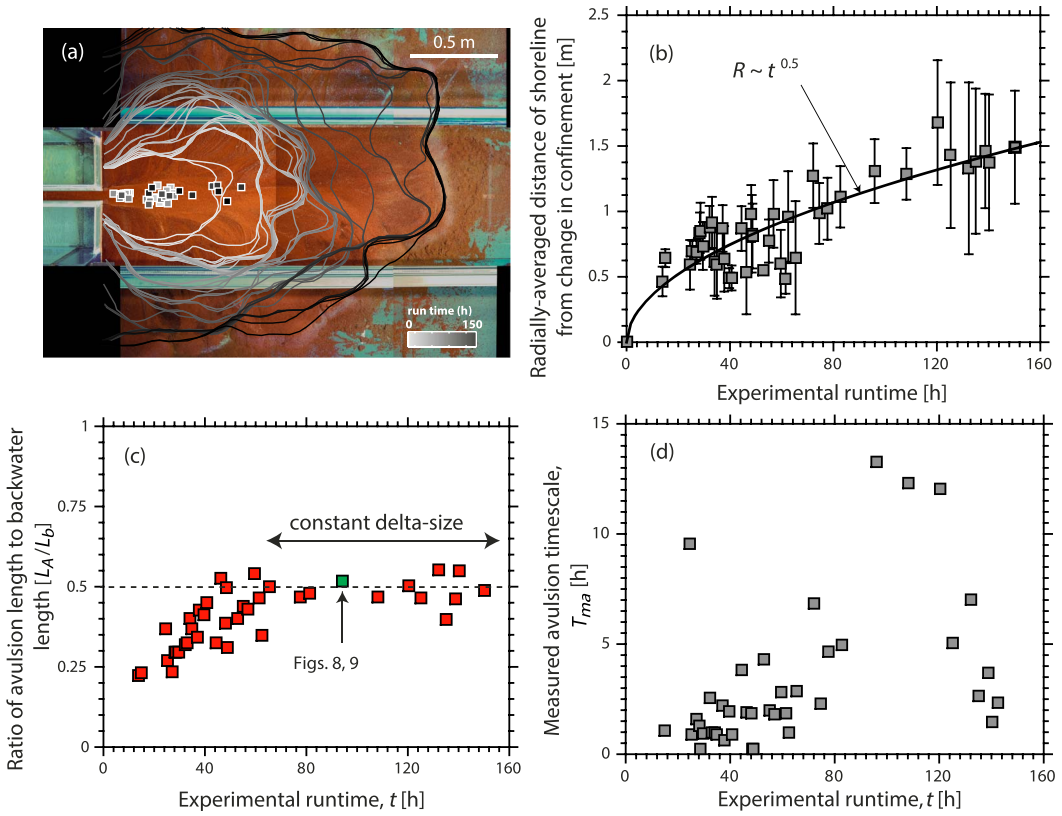

Figure 7. (a) Photograph of the experimental delta overlain with avulsion sites and shorelines through time. The avulsion sites and shorelines are graded from white to black in time. (b) Radially averaged distance of the shoreline (R) from the fixed reference frame of change of confinement in the experimental facility, which shows that the delta growth was well characterized by a functional form of square root of experimental runtime. The error bars denote the standard deviation of R resulting from spatial averaging of the shoreline location at a given instant of time. (c) Plot showing the temporal evolution of the ratio of the avulsion length (L_A) to the backwater length (L_b) where the avulsion length remained approximately constant after the delta reached an average size of $0.5L_b$ (data replotted from *Ganti et al.* [2016]). (d) Plot showing the temporal evolution of the measured avulsion timescale (T_{ma}) in the experiment.

3.2. Growth of the Experimental Delta Through Repeated Avulsions

The experimental delta grew through repeated avulsion cycles after approximately 13.9 h. During ~150 h of experimental runtime, we observed 41 river avulsions (Table 1). Figure 7a shows the avulsion locations overlain on a photograph of the experimental delta along with the evolution of the shorelines through time. Avulsions occurred in the vicinity of the location where the river exited the narrow section in our experimental facility for the first 66 h of the experiment. We quantified the growth of the experimental delta by measuring the radial distance of the shoreline from the fixed location of the change in confinement (R) in the experimental facility. The temporal growth of the radially averaged distance of the shoreline from the change in confinement was well characterized by the functional form: $R \sim t^{0.5}$, where t is the experimental runtime (Figure 7b)—an expected consequence from considerations of mass conservation for low-gradient deltas [*Swenson et al.,* 2000; *Powell et al.,* 2012]. Further, the lateral migration of the channels was not pronounced on the delta top and was limited to 2–3 times the typical channel width between avulsions, which led to the development of distinct lobes with each avulsion (Figure 7a). These results are akin to field observations of reduced channel migration and sinuosity within the backwater zone of the Mississippi River [*Hudson and Kessel*, 2000; *Lamb et al.,* 2012; *Nittrouer et al.,* 2012]. As the experimental delta grew larger, the avulsion sites translated seaward with the final set of avulsions occurring ~1.2 m downstream of the imposed change in confinement in our tank (Figure 7a), and we found that the avulsion lengths from this time onward (>66 h) scaled with the backwater length (Figure 7c) [*Ganti et al.,* 2016] similar to field observations [*Jerolmack and Swenson*, 2007; *Jerolmack*, 2009; *Chatanantavet et al.,* 2012; *Ganti et al.,* 2014].

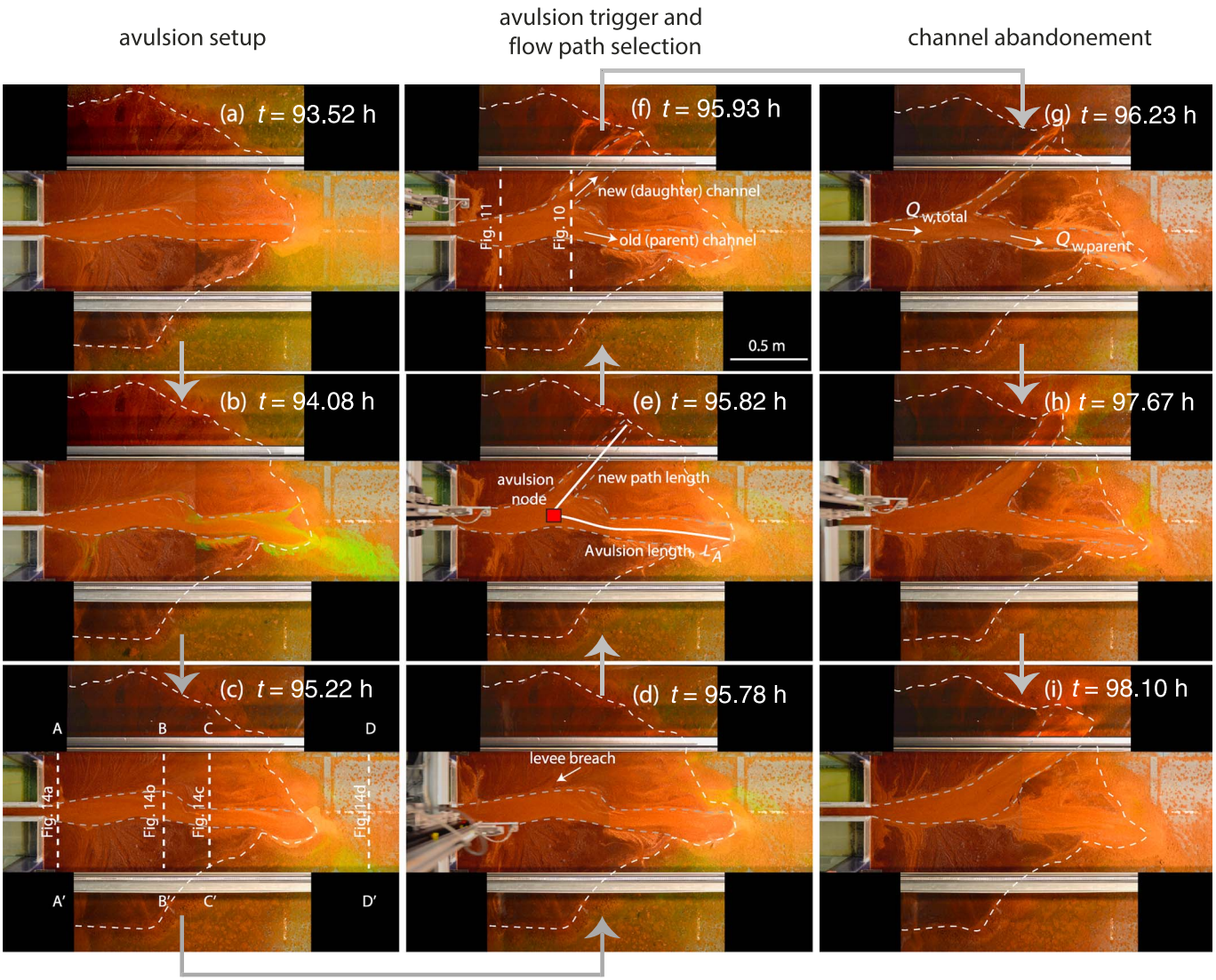

Figure 8. Photo sequence of an avulsion cycle in our experiment where the channel banks and the shoreline are indicated by dashed gray and white lines, respectively. (a–c) The initial phase of an avulsion setup where the parent channel resulted in progradation of the delta front, which resulted in aggradation within the channel. (d–f) After the channel was setup for an avulsion, a trigger event caused levee breach at the avulsion site, which was accompanied by flow path selection of the daughter channel. (g–i) The input water discharge was partitioned between the parent and daughter channels, and the flow through the parent channel progressively decreased resulting in the abandonment of the parent channel. The scale of the pictures is denoted in the lower right corner of Figure 8f. Figures 8d–8f are reproduced from *Ganti et al.* [2016].

The measured avulsion timescale describes the pace of the observed avulsion cycles in our experiment. The avulsion timescale (T_{ma}) in our experiment (Figure 7d) was variable with a mean and standard error of 3.45 ± 0.55 h. On average, the avulsions were more frequent during the early phase of delta growth (2.33 ± 0.54 h for experimental runtime less than 66 h) because the progradation rates were higher and consequently the aggradation rates were higher when compared to the later stage of delta growth (5.86 ± 1 h for experimental runtime greater than 66 h). The higher progradation rates during the early phase of delta growth are evident from the temporal evolution of the radial distance of shoreline from the fixed location of the change in confinement in the experimental facility (Figure 7b).

In the subsequent sections, we quantify the avulsion cycles considering the setup, trigger, path selection, and channel abandonment phases. Unless noted otherwise, all further analysis in this manuscript is focused on the backwater-controlled avulsions, i.e., avulsions that occurred at $t > 66$ h when the avulsion length was found to be approximately constant (Figure 7c), which constitutes 12 cycles. We present the ensemble

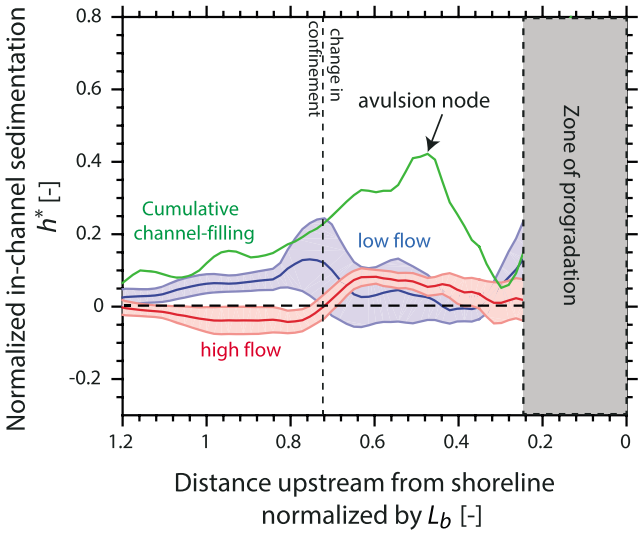

Figure 9. Plot showing the cumulative normalized channel-filling metric during the avulsion cycle shown in Figure 8 as a function of the streamwise distance upstream of the shoreline normalized by the backwater length (L_b = 2.87 m; Table 1). The red and blue lines denote the amount of normalized in-channel sedimentation during each high- and low-flow events, respectively, with the shaded region indicating the standard error that resulted from averaging across multiple flow events during the avulsion setup process. The green line is the cumulative in-channel sedimentation that occurred during the avulsion setup process (Figure 2), which shows that the in-channel sedimentation peaked within the backwater zone at the location coincident with the avulsion site. The distance upstream of the shoreline was measured from the shoreline at the time of the avulsion, and the gray shaded region shows the zone of progradation where vertical measurements of bed elevation change were not made.

statistics of avulsion cycles across all the backwater-controlled avulsions. In addition, we present detailed measurements and results for one avulsion cycle (Figure 8), which is representative of the avulsions observed for $t > 66$ h.

3.3. Avulsion Setup

Figure 9 shows the normalized channel-filling metric for the avulsion cycle example shown in Figure 8, which occurred at t = 95.91 h. Computation of the in-channel sedimentation within each flow event (Figure 9) reveals that during low flow, the spatial deceleration of the flow resulted in deposition in the upstream part of the backwater zone. In contrast, during high flows, incision originated near the shoreline and propagated upstream such that the net effect of multiple cycles of high and low flows was a peak in in-channel deposition at ~$0.5L_b$. These results are similar to the avulsion cycle that occurred at t = 125.33 h which was introduced in *Ganti et al.* [2016].

Figure 10a shows a comparison of the channel cross sections at the avulsion site for the avulsion cycle shown in Figure 8 where the in-channel deposition that preceded an avulsion is evident. Figure 10b shows the temporal evolution of the channel bed elevation at this avulsion site. We found that the channel bed elevation increased at the avulsion site, while the channel width and levee elevations were relatively constant through time (Figure 10b). The temporal evolution of the normalized channel-filling metric (h^*) indicates that the avulsion occurred when the in-channel sedimentation reached ~$0.42h_c$ (Figure 10c). Figure 10d shows the probability density function of the normalized channel-filling metric for the backwater-controlled avulsions during the experiment ($t > 66$ h; Figure 7c), which indicates that this value was variable across the observed backwater-controlled avulsions with a mean, mode, and standard deviation of 0.3, 0.24, and 0.13, respectively.

3.4. Avulsion Trigger

Of the 12 backwater-controlled avulsions, 9 avulsions (75%) occurred during high-flow events, and 3 occurred during low-flow events. This trend was similar across all the observed avulsions in our experiment. Of the 41 total avulsions, 32 avulsions (78%) occurred during high-flow events and 9 occurred during low-flow events (Table 1). We interpret this trend to reflect the higher propensity for high-flow discharge to initiate overbank flows, which increases the likelihood of triggering an avulsion [e.g., *Edmonds et al.,* 2009]. Figure 10a shows the channel cross section at the avulsion site before (black line) and after (red line) the avulsion event for the avulsion cycle shown in Figure 8. During the avulsion trigger event (high flow) the overbank flooding at the avulsion location resulted in a levee breach and formation of a new channel (Figures 8d–8f and 10a). Although overbank flows occurred during the experiment at locations other than the avulsion site, not all these overbank flows resulted in avulsions. For example, the crevasse splays shown in Figure 8 occurred near the location where the experimental alluvial river exited from the narrow section in the experimental facility; however, these splays were active only during the high flows and did not capture flow during the low-flow events.

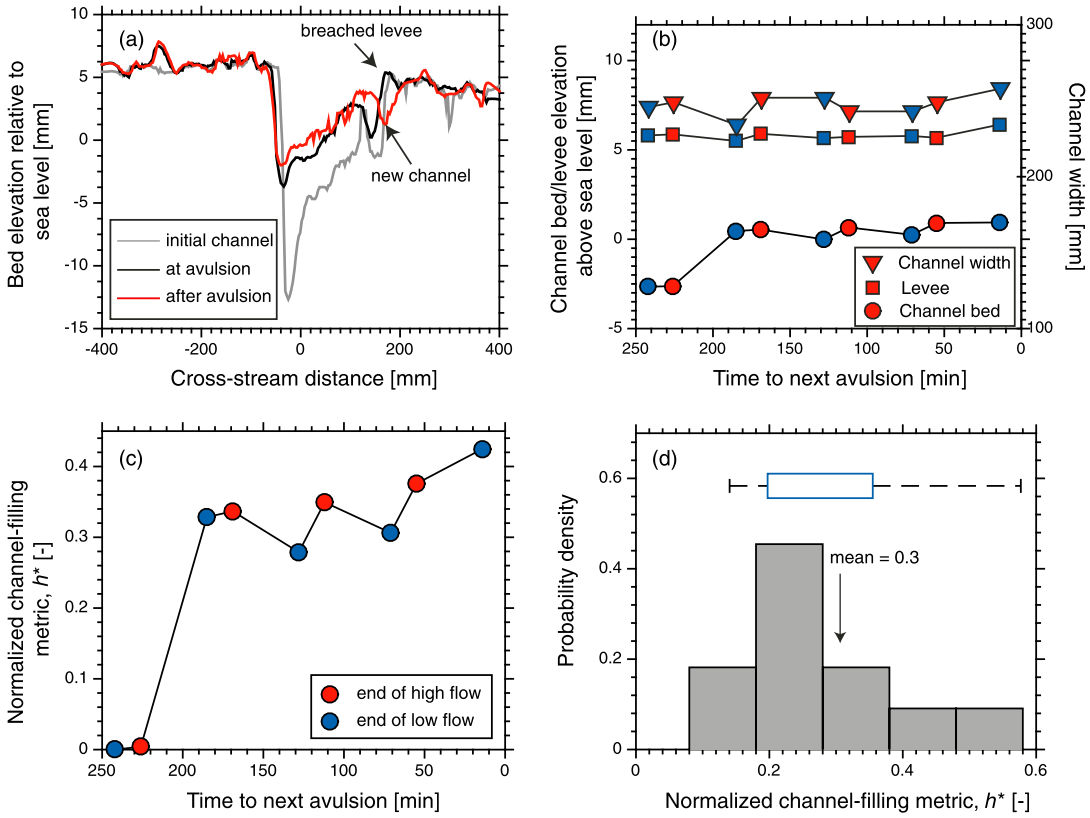

Figure 10. (a) Comparison of the channel cross section at the avulsion site for the avulsion cycle shown in Figure 8. The gray, black, and red lines indicate the channel cross section at the beginning of the avulsion cycle (Figure 8a), at the time of avulsion (Figure 8d), and just after the avulsion occurred (Figure 8f), respectively. (b) Temporal evolution of the channel bed elevation, levee elevation (vertical axis on the left), and channel width (vertical axis on the right) during the avulsion cycle indicates the deposition occurred at the avulsion site through the avulsion cycle. The red and blue markers indicate bed elevation, levee elevation, and channel widths at the end of high- and low-flow events, respectively. (c) Temporal evolution of the normalized channel-filling metric reveals that the critical value of h^* for the avulsion to occur in this case was 0.42. (d) Probability density function of h^* for all the backwater-controlled avulsions that occurred at $t > 66$ h. The edges of the blue box indicates the 25th and 75th percentiles of h^*, and the edges of the whiskers indicate 9th and 91st percentiles.

Following previous work [e.g., *Mohrig et al.,* 2000], we hypothesize that a given location has to be setup through channel bed deposition, prior to a trigger event, to cause an avulsion at that location. Figure 11a shows a comparison of the channel cross sections at the splay location during the avulsion cycle shown in Figure 8, and the temporal evolution of the channel bed elevation, channel width, and levee elevations is shown in Figure 11b. Results indicate that channel thalweg was subject to both erosion and deposition at the splay location during this avulsion cycle. Moreover, we found that the channel-filling metric (h^*) at the splay location and at the time of the avulsion (time = 0 on Figure 11c) was less than the channel-filling metric at the avulsion site at the same time (Figure 11c). The temporal evolution of the normalized channel-filling metric indicates that h^* at the splay location was never greater than h^* at the avulsion site during the setup process (Figure 11c). To test if this trend holds across all the backwater-controlled avulsions, we computed the normalized channel-filling metric at the location where the experimental river exits the narrow section in our experimental facility, which was the location where splays occurred frequently. Comparison of the normalized channel-filling metric at the time of avulsion for all the backwater avulsion and splay locations reveals that the in-channel sedimentation at the splay location was less than that at the avulsion location (Figures 9 and 11d). These observations suggest that the antecedent process of avulsion setup is crucial for overbank flows to produce an avulsion.

3.5. Flow Path Selection of the Daughter Channel

The diversion of flow from the parent channel was accompanied by selection of a new flow path on the delta top. We quantified the flow path selection of the daughter channels by measuring the linear distance between the avulsion site and all points along the shoreline. Figure 12a shows the probability density

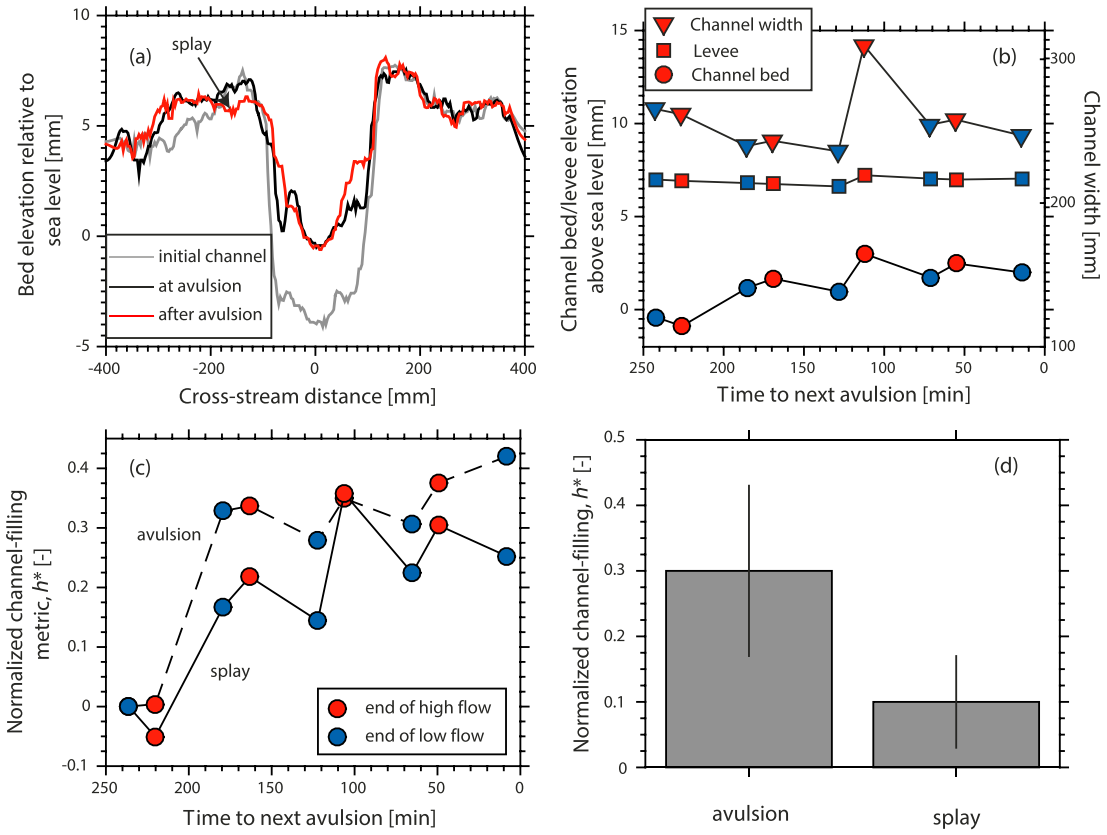

Figure 11. (a) Comparison of the cross-sectional topography at the location of crevasse splays for the avulsion cycle shown in Figure 8. (b) Temporal evolution of the channel bed elevation, levee elevation (vertical axis on the left), and channel width (vertical axis on the right) at the location of crevasse splay indicates that thalweg erosion and deposition occurred through the avulsion cycle. (c) Temporal evolution of h^* indicates that this value is never greater than the h^* value at the avulsion site during the avulsion setup process. The dashed line in this plot is reproduced from Figure 10c. (d) Comparison of the normalized channel-filling metric at the time of an avulsion for both the avulsion site and the splay location across all the backwater-controlled avulsions. The black lines indicate standard deviation of h^*.

function of all the possible flow paths from the avulsion site to the shoreline for the avulsion cycle shown in Figure 8. We measured the linear distance between the avulsion site to the river mouths of both the parent and daughter channels, which we term "old path length" and "new path length," respectively. For the avulsion cycle shown in Figure 8, we found that the old path length was one of the longest possible paths (90th percentile), whereas the new path length was one of the shortest possible paths (20th percentile) to the shoreline (Figure 12a). To test if this difference is statistically significant for all avulsions, we computed the probability density function of all possible flow paths at the time of each avulsion and then computed the percentile values of the new path length and old path length (Figure 12b). We find that the new path length was consistently one of the shortest paths to the shoreline from the avulsion site (median across avulsions was 25th percentile), and the old path length was one of the longest possible paths to the shoreline from the avulsion site (median across avulsions was 75th percentile).

We compared the new path length to the median of all the possible path lengths, both normalized by the old path length, which is shown in Figure 12c. Results show that the new path length was consistently shorter than the old path length, which is evidenced by the data plotting in the region with abscissae less than 1 with the exception of three points (Figure 12c). Further, the median of all path lengths, which is the 50th percentile of all possible path lengths, is consistently less than the old path length, which is evidenced by the data plotting in the region with ordinate values less than 1 with the exception of five data points (Figure 12c). Moreover, this trend holds for both the backwater-controlled avulsions and the bed slope-mediated avulsions that occurred early during the experiment, i.e., $t < 66$ h.

Finally, Figure 12d shows a plan view of the pairs of parent (solid lines) and daughter channel paths (dashed lines) for all the avulsions. Visual inspection reveals that the channel flow paths cover the whole deltaic plain

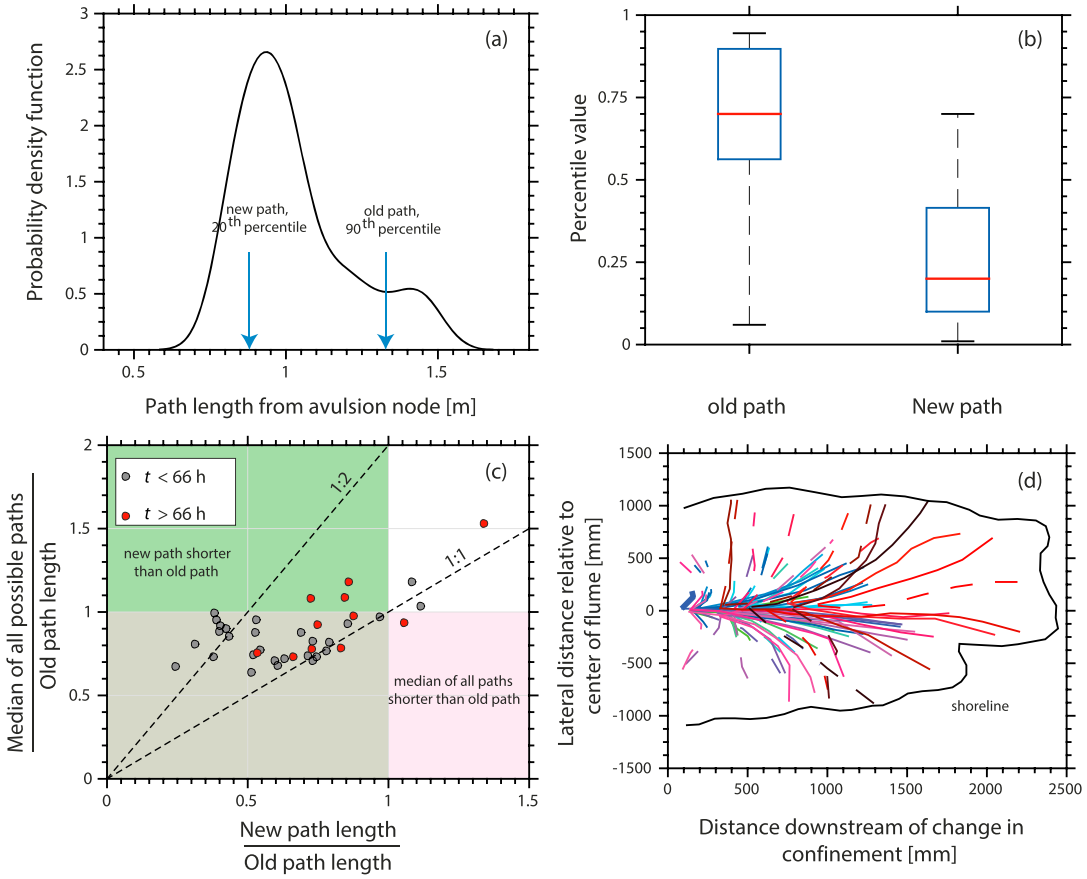

Figure 12. (a) Probability density of all possible flow paths from the avulsion site to the shoreline indicated in Figure 8e. The new path length and old path length were the 20th and 90th percentiles of all possible flow path lengths to the shoreline. (b) Box and whisker plot showing the percentile values of the old and new path lengths for all avulsions during the experiment. (c) Plot comparing the median of all possible path lengths to the new path length where both these quantities were normalized by the old path length. Backwater-controlled ($t < 66$ h) and bed slope-mediated avulsions ($t > 66$ h) are indicated by red and gray markers, respectively. The shaded green and pink areas demarcate the phase space where the new path length is shorter than old path length and the median of all possible path lengths is shorter than old path length, respectively, and the shaded brown area indicates where both of the above conditions are satisfied. (d) Plan view of the pairs of new path (dashed line) and old path (solid line) for all the avulsions during the experiment qualitatively indicates that channelization occurred across the whole deltaic plain.

with no preferential clustering of channel paths. Because the delta top was always channelized at some point during the experimental run, there was reoccupation of flow paths from previous avulsion cycles; however, our data do not show preferential clustering of channels on the delta top, which may be a result of the lack of floodplain aggradation and sediment cohesion in our experiment.

3.6. Abandonment of the Parent Channel

The channelization of flow into the daughter channel was accompanied by abandonment of the parent channel in our experiments. In most cases, the parent channel abandonment was abrupt and occurred within the same or the subsequent flow event in which the avulsion occurred. This did not allow for quantification of the mechanics of channel abandonment for all the avulsions because data of bed evolution were collected at the end of each flow event. The avulsion cycle shown in Figure 8 was one of the few avulsions where the parent channel was active for ~2 h after the avulsion occurred, which was approximately 15% of the time before the next avulsion occurred. We quantified the mechanics leading to the abandonment of the parent channel in this case by measuring both the flow partitioning between the parent and daughter channel and also the bed elevation evolution of the parent channel after the avulsion occurred.

We computed the water surface velocities along the parent channel upstream and downstream of the avulsion site using the overhead dye videos. We then computed the cross-sectional area along the thalweg

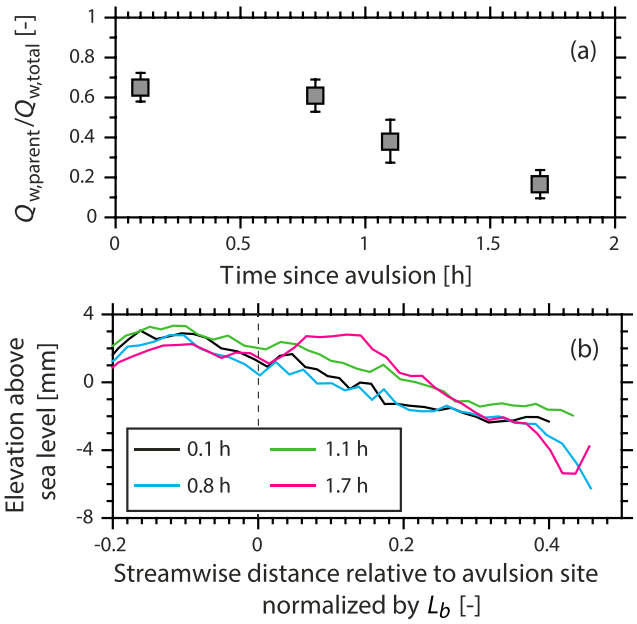

Figure 13. (a) Plot showing the temporal evolution of the ratio of the water discharge through the parent channel to the water discharge upstream of the avulsion site (section 3.6; Figure 8g). (b) Topographic evolution of the cross-section-averaged bed elevation along the parent channel for the avulsion cycle shown in Figure 8, which highlights the deposition within the parent channel immediately downstream of the avulsion site. Different colors indicate bed profiles at different times since the avulsion occurred.

of the parent channel from the 3-D bed scans that were collected at the end of each flow event. The product of the computed cross-sectional area and the water surface velocity at a given location yielded an estimate of the water discharge through the parent channel; however, we note that this an overestimate of the actual water discharge because the water surface velocity is higher than the depth-averaged flow velocity. To quantify the flow partitioning between the parent and the daughter channel, we averaged the estimates of water discharges upstream and downstream of the avulsion site along the thalweg of the parent channel. We then computed the ratio of the water discharge downstream of the avulsion site along the parent channel ($Q_{w,\mathrm{parent}}$) to that of the estimated water discharge upstream of the avulsion site ($Q_{w,\mathrm{total}}$; Figure 8g). Because the water discharge from upstream of the avulsion site is conserved between the parent and the daughter channels, this procedure yielded an estimate of the temporal evolution of the flow partitioning between the parent and the daughter channel. Results indicate that the daughter channel progressively captured more flow from upstream until there was no more flow into the parent channel, which resulted in a decline in the proportion of the total flow through the parent channel (Figures 13a and 8g–8i).

Figure 13b shows the temporal evolution of the cross-section-averaged bed elevation along the parent channel, which was computed using equation (2). The channel bed elevation increased downstream of the avulsion site suggesting that the decrease in flow through the parent channel (Figure 13a) was accompanied by deposition within the parent channel. For this avulsion cycle, the in-channel sedimentation downstream of the avulsion site was particularly pronounced from 1.1 to 1.7 h after the avulsion occurred (Figure 13b). The spatial decrease in water discharge through the parent channel led to a decrease in sediment transport capacity, which caused deposition within the parent channel downstream of the avulsion site. It is likely that in other avulsions the daughter channel captured majority of the incoming water discharge more rapidly, which led to more abrupt abandonment of the parent channel. Importantly, despite the timescale of abandonment being relatively long for the avulsion cycle in Figures 8 and 13, the parent channel was only filled with sediment in the region immediately downstream of the avulsion site, and the remnant of the parent channel bed is evident in the lowermost portions even after channel abandonment (Figure 13).

3.7. Experimental Stratigraphy

To assess how the avulsion cycle is recorded in the sedimentary strata, we constructed the synthetic stratigraphy using time series of topographic data in our experiment. Avulsions are often inferred in the stratigraphic record as processes that lead to the formation of discrete lenses of sandstone inferred to be channel belts that were abandoned by avulsions. In this interpretation, the internal stratigraphy of the channel body may contain information about the in-channel sedimentation that led to setup prior to an avulsion. For example, *Mohrig et al.* [2000] inferred that channel bodies composed of multiple stories suggest an avulsion setup in which in-channel deposition is onefold to threefold the channel depth. Here we evaluate these ideas

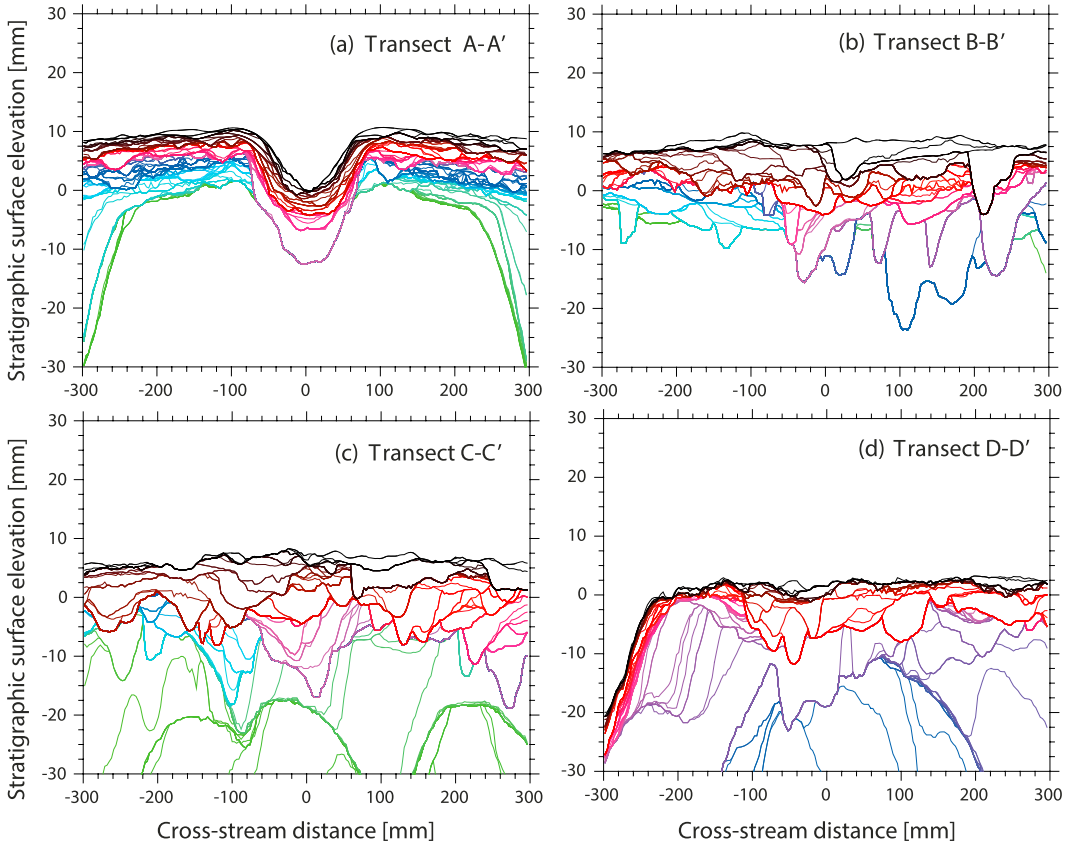

Figure 14. Strike-oriented synthetic stratigraphy constructed from elevation time series at four locations along the delta surface (see Figure 8c). (a–d) The four transects were perpendicular to the longitudinal axis of the flume and were 10 cm, 90 cm, 110 cm, and 180 cm downstream of the imposed change in confinement of the experimental facility. The erosional boundaries are color coded from green to black, with the erosional boundaries in green being stratigraphically oldest and the erosional boundaries in black being stratigraphically youngest.

using synthetic stratigraphy. Figure 14 shows the strike-oriented, synthetic stratigraphic sections at four locations along the delta top, which were 10 cm (transect A-A′; $0.035L_b$), 90 cm (transect B-B′; $0.31L_b$), 110 cm (transect C-C′; $0.38L_b$), and 180 cm (transect D-D′; $0.63L_b$) downstream of the change in confinement in the experimental facility (Figure 8c). Transect A-A′ coincided with the axial plane of avulsions during the early phase of delta growth, transects B-B′ and C-C′ coincided with the axial plane of avulsions during the later stage of delta growth, and transect D-D′ was downstream of the avulsion sites (Figures 7a and 8c). Each line represents a preserved erosional surface, color coded in stratigraphic order (or time), which are inferred to separate distinct sedimentary beds in between.

Transect A-A′ represents the location where the river exits the narrow section in the experimental facility, and consequently the channel was located along the centerline of the flume at all times during the deltaic evolution (Figure 14a). The synthetic stratigraphy at this location shows beds bounded by erosional surfaces within the channel body that resulted from depositional and erosional events during low- and high-flow events, respectively. Results also show that channelized deposits were stacked within a deeper valley, which resulted—on independent evidence from surface evolution observations—from erosion induced from river shortening due to an avulsion. Stratigraphy on the flanks of the main channel was created through channelization during early phase of the experiment, and crevasse splays during the later stage of the deltaic evolution when a channel did not visit these locations. The primary component of flow directions for splays was parallel to the stratigraphic section A-A′. Synthetic stratigraphy at transects B-B′ and C-C′ show stacked channel bodies across the whole stratigraphic section because these locations were channelized at some point during the deltaic evolution, and the primary component of flow direction was perpendicular or oblique to the stratigraphic sections (Figures 14b and 14c). The reoccupation of

previously channelized locations at these transects resulted in the formation of the superimposed, incised channel bodies. Lateral migration of the channel may result in each story of the incised channel body to comprise bar accretion surfaces; however, the temporal resolution of the topographic scans (one scan at the end of each flow event) did not allow us to resolve these surfaces in the synthetic stratigraphy. Because our experiment did not contain subsidence and floodplain depositional processes, the channel bodies were not separated in their spatial extent. These channel bodies are separated by overbank mudstone in some natural examples [e.g., *Mohrig et al.,* 2000]. At transect D-D′ (Figure 14d), the majority of the stratigraphy was dominated by the submarine, clinoform strata and the density of stacked channel-bodies is reduced when compared to synthetic stratigraphy at transects B-B′ and C-C′ (Figures 14b and 14c).

Visual inspection of the synthetic stratigraphy reveals that the density of multistory channel bodies is high around the avulsion sites with these features spanning the whole cross section at transects B-B′ and C-C′ (Figure 14). This could be a direct result of avulsing channels reoccupying old channel paths [e.g., *Mohrig et al.,* 2000; *Chamberlin and Hajek*, 2015], although in our experiment all the locations along each transect were channelized because of the lack of fine-sediment deposition on the floodplain. We quantified the downstream change in stratigraphic architecture by computing the bed thicknesses from the synthetic stratigraphy, which were defined as the thickness of the deposit preserved between two successive erosional boundaries (Figure 14). We computed bed thicknesses from the portion of the stratigraphic section that was always a part of the delta top, i.e., we did not measure the thickness of the beds within the clinoform strata.

Figure 15a shows the statistics of bed thickness normalized by the normal-flow depth of the low flow (Table 1) as a function of distance from the change in confinement in the experimental facility normalized by the backwater length. Results indicate that the mean and median of the normalized bed thickness show a general increase as we move downstream from the change in confinement in our experimental facility. This trend holds until a distance of ~$0.52L_b$ (150 cm) beyond which there is a decrease in the mean and median of the normalized bed thickness. The highest values in the normalized bed thickness approximately coincide with the locations where avulsion density was high (Figures 15a and 15b). Our results indicate that the amount of in-channel sedimentation required for avulsions (Figure 10d) was approximately equal to the mean normalized bed thickness (Figure 15a). Moreover, our results indicate that the amount of in-channel sedimentation is likely to peak at the avulsion sites, and this value may be underestimated when measured away from the avulsion sites.

In our experiment, the aggradation on the delta topset was a result of progradation of the delta front [e.g., *Paola*, 2000] because there was no externally imposed subsidence or base-level rise. Figure 7b shows that the progradation rate decreased with experimental runtime, and this should be accompanied by decrease in aggradation rates, which will reduce the preservation potential of surface dynamics in the stratigraphic record. The thickness of the deposits shown in Figures 14b and 14c shows a qualitative decrease as we move stratigraphically up. This observation was quantified by comparing the statistics of normalized bed thickness for different time intervals ($t < 66$ h and $t > 66$ h) for the stratigraphic sections at transects B-B′ and C-C′. Figure 15c shows that the mean normalized bed thickness was slightly lower for stratigraphically younger deposits ($t > 66$ h) when compared to the stratigraphically older deposits ($t < 66$ h), which is likely a result of reduced progradation rates and consequently reduced aggradation rates.

4. Discussion

4.1. The Avulsion Cycle on Backwater-Controlled Deltas

Our experimental results indicate some differences for backwater-influenced deltas in the mechanics leading to a lobe-scale avulsion as compared to recent theory (Figure 16) [e.g., *Edmonds et al.,* 2009; *Hoyal and Sheets*, 2009]. Our results indicate that the in-channel sedimentation peaks within the backwater zone resulting in a preferential location for the avulsion to occur (Figure 16b). Although our study cannot unequivocally discard the possibility that backwater-controlled avulsions may occur under steady discharge conditions, our results confirm theory and numerical modeling [*Chatanantavet et al.,* 2012], which show that this preferential avulsion node emerges when the alluvial river is in a state of perpetual morphodynamic disequilibrium within the backwater zone owing to flood discharge variability. The mechanics of backwater-controlled avulsion setup are in contrast to the experiments on cohesive deltas

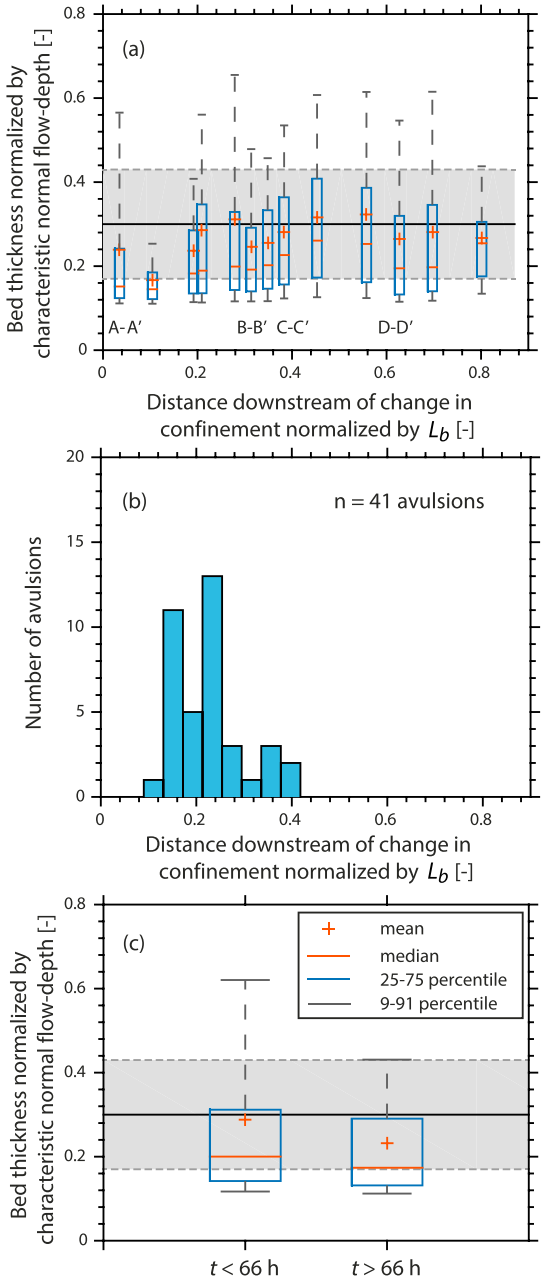

Figure 15. Plots showing the computed statistics of bed thicknesses normalized by the normal-flow depth of the low flow. (a) The mean and the median of the normalized bed thickness increased with downstream distance from the change in confinement until a distance of $0.52L_b$ (150 cm) and then decreased with downstream distance. (b) Density of avulsion sites as a function of downstream distance from the change in confinement in our experimental facility normalized by $L_b = 2.87$ m. (c) Comparison of the normalized bed thickness statistics for stratigraphically older ($t < 66$ h) and younger ($t > 66$ h) deposits reveals that the preservation potential of the surface dynamics in the stratigraphy was slightly higher early in the experiment because of relatively high aggradation rates when compared to the later stage of the experiment. The shaded region in both the panels shows the mean (black line) and standard deviation (dashed gray line) of h^* (Figure 10d).

by *Hoyal and Sheets* [2009], where mouth bar deposition near the shoreline led to an upstream migrating flow disturbance, which resulted in backfilling of the channel (Figures 1 and 16) [e.g., *Edmonds et al.,* 2009]. This backfilling, in turn, led to increased overbank flows, rapid bed and levee aggradation, and superelevation of the channel above its surrounding floodplains that rendered the channel unstable and poised for an avulsion [*Hoyal and Sheets*, 2009]. The in-channel backfilling during an avulsion cycle was also observed in physical experiments on fan and fan-delta evolution [e.g., *van Dijk et al.,* 2009; *Reitz and Jerolmack,* 2012; *Hamilton et al.,* 2013]. The similarity of our findings and those of *Hoyal and Sheets* [2009] [and also *van Dijk et al.,* 2009; *Reitz and Jerolmack,* 2012; *Hamilton et al.,* 2013] lies in the fact that both our mechanisms for driving avulsions are fundamentally controlled by the downstream boundary condition, which is in contrast to topographically controlled avulsions on fans and fan-deltas [*Ganti et al.,* 2014]. It is likely that the "morphodynamic backwater effects" of *Hoyal and Sheets* [2009] (note that this is different from the classical use of the term "backwater" resulting from nonuniform flow hydrodynamics), which resulted from cohesive sediment, and the backwater hydrodynamics presented in this manuscript both may be at play in natural systems. However, our results suggest that the upstream migrating wave of deposition is unlikely to persist in natural, low-gradient deltaic systems with persistent backwater hydrodynamics because erosion preferentially occurs within the downstream portion of the backwater zone during high flood discharges. Instead, lobe-scale avulsions appear to be setup by a

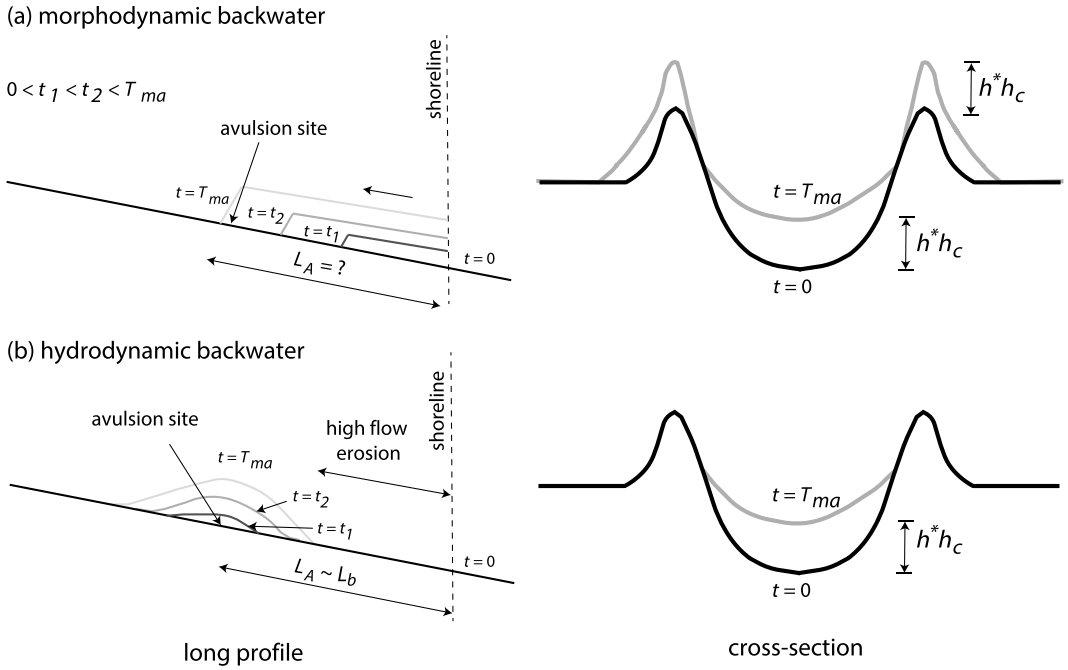

Figure 16. Schematic summary of the key differences between the existing theory ((a) morphodynamic backwater) for avulsion cycles and the backwater-controlled avulsion cycles. The first and the second columns of the figure represent the schematic long profile of the river and the channel cross section at the avulsion site, respectively. (a) The morphodynamic backwater results in an upstream migrating wave of aggradation and in-channel backfilling that initiates near the shoreline as a result of mouth bar stagnation. The channel bed and the levees aggrade at the avulsion site resulting in superelevation of the levees above the surrounding floodplain, which triggers an avulsion. (b) Backwater-controlled avulsions are setup by enhanced in-channel sedimentation within the upstream portion of the backwater zone, which results from the preferential erosion caused by the floods in the downstream portion of the backwater zone. This enhanced in-channel sedimentation results in an avulsion setup, which is maximum at a characteristic distance upstream of the shoreline and is higher than channel aggradation elsewhere along the channel bed. The channel bed aggrades at the avulsion site; however, levees do not aggrade significantly because the variable flows within the backwater zone are accommodated by changing water surface slope with little changes in water stage height that may result in overbank deposition.

downstream migrating wave of deposition during low flood discharges, which is modulated by upstream migrating wave of incision that initiates at the shoreline during high flood discharges (Figure 16b), resulting in a hump of in-channel sedimentation rather than an upstream migrating wave [*Chatanantavet et al.,* 2012; *Ganti et al.,* 2016]. This notwithstanding, smaller-scale avulsions do occur within the delta lobe complex, which are commonly referred to as intradelta avulsions [*Coleman and Gagliano*, 1964; *Edmonds et al.,* 2009; *Hoyal and Sheets*, 2009]. These avulsions may be influenced by flow disturbances and the morphodynamic backwater effects arising from mouth bar deposition and stagnation as suggested by *Hoyal and Sheets* [2009] and *Edmonds et al.* [2009].

The critical in-channel sedimentation required for the occurrence of avulsions was ~0.3h_c in our experiments (Figure 10d), and the in-channel sedimentation peaks within the backwater zone during an avulsion cycle [*Ganti et al.,* 2016]. This value measured from our experiment is less than those observed previously from stratigraphic observations [*Mohrig et al.,* 2000] and scaling results from experimental and field data [*Jerolmack and Mohrig*, 2007], which tend to have an average value near unity. Previous workers have shown that the in-channel sedimentation thickness (equation (1)), when combined with an estimate of net aggradation rate and channel depth, provides a good approximation of the mean avulsion timescale over multiple avulsion cycles (i.e., $T_{ma} \sim h^* h_c / v_A$) [*Jerolmack and Mohrig*, 2007] with evidence for positive correlation between avulsion frequency and net aggradation rate from both experimental [*Bryant et al.,* 1995; *Ashworth et al.,* 2004; *Martin et al.,* 2009] and field studies [*Törnqvist*, 1994; *Stouthamer and Berendsen*, 2001; *Jain and Sinha*, 2003]. Thus, all else equal, our experiments indicate more frequent avulsions than in other studies, which might be due to variable flow discharges in our experiments [e.g., *Edmonds et al.,* 2009; *Ganti et al.,* 2014]. To test this idea, we compared our experimental results ($h^* = 0.3$

and coefficient of variation of stage height = 0.22, which is computed as the ratio of the standard deviation to the mean) with the compilation of dimensionless avulsion timescale across fans and deltas from *Ganti et al.* [2014]. This comparison suggests that the water stage height variability may indeed play an important secondary role in setting the timescale of avulsions [*Ganti et al.,* 2014, Figure 3d] with avulsions happening more frequently than expected by channel-filling theory in stormier environments, i.e., systems that have high flood discharge variability.

Further, the avulsion trigger in our experiment was predominantly the short timescale, high discharge floods (Table 1), which resulted in overbank flooding and levee breaches. This observation is consistent with previous work that highlighted that avulsions (on deltas or otherwise) are triggered during high flood discharges [e.g., *Mosley*, 1975; *Brizga and Finlayson*, 1990; *Slingerland and Smith*, 1998; *Mohrig et al.,* 2000; *Edmonds et al.,* 2009; *Reitz et al.,* 2010]. Importantly, in-channel sedimentation, as opposed to building of levees above the surrounding floodplain, was the primary process of avulsion setup in our experiments (Figure 16). Sediment was in intermittent suspension in our experiment (Table 1), which led to marginal overbank deposition and development of levees. Overbank flows in the lower part of the backwater zone were limited, which is expected because changes in water surface elevation are muted within the backwater zone such that high flood discharges are accommodated by steepening water surface slopes rather than through increased stage height [*Lamb et al.,* 2012; *Nittrouer et al.,* 2012]. The lack of cohesive sediment and vegetation might also have limited the importance of levees in our experiment.

In our experiment, flow paths of the daughter channel were consistently one of the shortest paths to the shoreline, and we did not observe significant preferential clustering of channel paths over multiple avulsion cycles (Figure 12). This is likely a result of the lack of fine sediment and floodplain aggradation in our experiment. Previous workers have argued that channel reoccupation occurs because noncohesive channel sediments are readily erodible when compared to muddy floodplains [*Aslan et al.,* 2005]. Further, recent experimental and numerical models suggest that the tendency of channels to reoccupy their former paths is determined by the competition between channel reactivation by reoccupation (determined by avulsion frequency) and abandoned-channel annealing by floodplain deposition of fine sediment [*Reitz et al.,* 2010]. Although the lack of grain size variation may have direct implications for the absence of channel clustering in our experiment, *Reitz et al.* [2010] noted that the presence of mud in lowland deltas may result in fast annealing of abandoned channels and thus less persistent channel networks across the deltaic plain, similar to our experimental results. Moreover, channel abandonment in our experiment occurred through sediment deposition within the parent channel immediately downstream of the avulsion site (Figure 13), which may likely reduce preferential reoccupation of the previous flow paths despite the downstream portions of the parent channels being unfilled by sediment.

Abandonment of the parent channel was abrupt in most of the avulsion cycles in our experiment, and this was consistent across both the bed slope-mediated (early phase of delta growth) and backwater-controlled avulsions (later phase of delta growth). Previous workers have studied the stability of channel bifurcations in deltaic systems [*Kleinhans et al.,* 2011; *Edmonds*, 2012]. In particular, *Edmonds* [2012] described the stability of backwater-influenced river bifurcations in the context of Mississippi-Atchafalaya system. *Edmonds* [2012] noted that the Mississippi River captures flow from the Atchafalaya during low flood discharges because of steeper water surface slope at the bifurcation node and vice versa at high flows, thus leading to the enhanced stability of the bifurcation. This mechanism for enhanced stability of bifurcations did not appear to occur in our experiments, perhaps due to smaller differences in the relative channel lengths in our experiment as compared to the Mississippi River. For example, the Mississippi River downstream of the Atchafalaya bifurcation is twice as long as the Atchafalaya River, whereas for the backwater-controlled avulsions in our experiment, the ratio of the length of the daughter and parent channel was typically greater than 0.5 (red points in Figure 12c). However, for the avulsion cycle shown in Figure 8, the ratio of the path length of daughter channel to parent channel was ~0.6 and the parent channel abandonment was more gradual in this example. The timescale of abandonment of the parent channel for this avulsion cycle (~$0.15T_{ma}$) is consistent with the numerical predictions of *Edmonds* [2012], where the prediction of the timescale of abandonment of Mississippi River (parent channel) was ~300 years (~$0.24T_{ma}$).

Tides are another important natural phenomenon that is not modeled in our experiments and can potentially affect the hydrodynamics within the backwater reach [e.g., *Hoitink and Jay*, 2016] even under

microtidal conditions [e.g., *Leonardi et al.*, 2015]. The backwater length scaling of delta lobe size across a wide variety of deltaic environments [*Jerolmack and Mohrig*, 2007; *Chatanantavet et al.*, 2012; *Ganti et al.*, 2014, 2016] suggests that the tidal influence on avulsion location may be secondary to river floods owing to the short timescales of morphodynamic adjustment induced by tides when compared to the avulsion timescales on many low-gradient deltas. For example, the duration of tides may be short enough when compared to timescales of floods such that a typical M1 and M2 flood event may comprise several tidal cycles. Tidal influence, however, may be significant in filling abandoned channels, which affects the channel reoccupation and abandonment dynamics over long timescales.

4.2. Implications for Hazard and Delta Management

Our results provide a mechanistic underpinning for the observed correlation between avulsion length and the backwater length on low-gradient deltas [*Jerolmack and Mohrig*, 2007; *Jerolmack*, 2009; *Chatanantavet et al.,* 2012; *Ganti et al.,* 2014], thus providing an expectation for the most likely location of lobe-scale avulsions on river deltas. Importantly, in-channel deposition peaks within the upstream portion of the backwater zone during an avulsion cycle (Figure 16b). Thus, field monitoring of the channel bed elevation within the upstream portion of the backwater zone of coastal rivers may give insight into the most likely location for future avulsions and may be used for prospective early-warning signals for impending avulsions. Further, we find that flow path selection on river deltas may be less predictable than previously thought [*Reitz et al.,* 2010], highlighting the hazard associated with avulsions for communities living on deltas worldwide.

Backwater-mediated avulsion sites on river deltas can spatially move upstream or downstream with changing boundary conditions. For example, given relatively constant backwater length, avulsion sites may translate upstream during relative sea level rise and vice versa. Changes in hydrologic regime of deltas influenced by anthropogenic interference or climate should change the length scale over which backwater and drawdown effects manifest, thus influencing the likely location of avulsions on river deltas. In addition, avulsions might occur more frequently in locations where the climate shifts toward more extreme events [e.g., *Donat et al.,* 2016]. Finally, quantitative knowledge of avulsion location and timescale should be helpful for mitigating hazards associated with land loss through engineering strategies [e.g., *Kim et al.,* 2009].

4.3. Implications for Interpreting Avulsions in the Rock Record

Our results indicate that channel-fill thickness estimated from synthetic stratigraphy (Figure 15) does recover, on average, the critical in-channel sedimentation required for avulsions to occur in our experiment. This confirms the use of depositional patterns at outcrop scale to decipher avulsion thresholds [*Mohrig et al.,* 2000]. Importantly, we found that in-channel sedimentation peaks within the backwater zone at the avulsion site (Figure 9), and in-channel sedimentation is lower than this value everywhere else within the backwater zone [*Chatanantavet et al.,* 2012; *Ganti et al.,* 2016]. At the outcrop scale, this observation indicates that the in-channel sedimentation should be measured over long distances in the paleo-flow direction to infer the peak value and the possible location of ancient avulsion sites (Figure 15). For example, avulsion setup thresholds are likely underestimated if measurements are made away from the paleo-avulsion site. Additionally, previous workers have interpreted channel-fill strata as a consequence of deposition during the waning phase of channel abandonment [*Mohrig et al.,* 2000; *Slingerland and Smith*, 2004]; however, our results indicate that in-channel sedimentation is the driver of avulsions in backwater-controlled deltas—a result consistent with the experimental observations of *Hoyal and Sheets* [2009]. Moreover, backwater-controlled avulsions can occur with little change in levee superelevation height [cf. *Mohrig et al.,* 2000] because the backwater zone is characterized by little variations in water stage heights (Figures 10a and 16) [e.g., *Lamb et al.,* 2012; *Nittrouer et al.,* 2012].

The density of channel-body clustering is high around the avulsion sites compared to the channel-body clustering downstream of avulsions (Figure 14). Although floodplain deposition of fine sediment was absent in our experiment, these results indicate that the channel-body clustering may give insight into the location of paleo-river avulsions in deltaic deposits [e.g., *Jerolmack and Paola*, 2007; *Hajek et al.,* 2012]. Our experimental results of avulsion length scaling with the backwater length (Figure 7c) also bolster the use of backwater length as a paleohydraulic reconstruction tool [*DiBiase et al.,* 2013] where the avulsion length, channel bed slope, and characteristic flow depth are interrelated, i.e., $L_A \sim L_b = h_c/S$. Given estimates of characteristic flow depth and paleo-slopes from outcrop observations [e.g., *Paola and Mohrig*, 1996; *Petter*, 2010; *Lynds et al.,* 2014;

Trampush et al., 2014], one can make a first-order prediction of the location of paleo-avulsions using the estimated backwater length. Further, given observations of inferred avulsion sites within the rock record [e.g., *Mohrig et al.,* 2000; *Chamberlin and Hajek*, 2015], the backwater length scale can be used to infer the location of paleo-shorelines.

5. Conclusions

We presented results from the first laboratory delta that grew through repeated cycles of lobe growth and channel avulsion under the influence of persistent backwater hydrodynamics achieved through variable flood discharges and subcritical flows. Our work demonstrates that backwater and drawdown hydrodynamics significantly affect the patterns of erosion and deposition within the backwater reach and result in avulsion sites that occur at a characteristic distance upstream of the shoreline, which scales with the backwater length. Backwater-controlled avulsions are setup by in-channel deposition that peaks ($h^* = 0.3 \pm 0.13$) within the upstream portion of the backwater zone and is fundamentally a result of patterns of erosion and deposition driven by multiple flood events of different discharge. We found that in-channel sedimentation as opposed to levee superelevation was the first-order control on occurrence of backwater-controlled avulsions, with avulsions being triggered most of the time during high flood discharges (78% of avulsions) through overbank flooding and levee breach. The new flow path was consistently one of the shortest paths to the shoreline with no evidence for preferential reoccupation of the flow paths from previous avulsion cycles likely due to the absence of fine sediment and floodplain depositional processes. Channel abandonment was rapid and occurred through sedimentation within the parent channel immediately downstream of the avulsion sites both prior to and following the avulsion. Experimental synthetic stratigraphy revealed that the bed thickness measurements were highest around the avulsion sites and low elsewhere reflecting the depositional setup processes of backwater-controlled avulsions. Altogether, this work gives new insight into understanding future avulsions—including their timing, location, and path selection—on backwater-mediated deltas, as well as reconstructing avulsion node and shoreline locations from ancient deltas based on backwater length scaling relations.

Acknowledgments

We thank Brian Fuller for assistance in conducting the experiments and Kirby Sikes for assistance in analysis of the dye videos. Critical and constructive reviews by David Hoyal and two anonymous reviewers on an earlier draft improved the presentation of this work. M.P.L. acknowledges support from National Science Foundation (grants OCE-1233685 and 1427177), the California Institute Technology Terrestrial Hazards Observations and Reporting Center (THOR) program made possible by Foster and Coco Stanback, and the Royal Academy of Engineering Distinguished Visiting Professor Fellowship from the Imperial College London. V.G. acknowledges further support from NCED2 Synthesis Postdoctoral Fellowship, and the Imperial College London Junior Research Fellowship. Data used in this manuscript are available upon request from V.G. (v.ganti@imperial.ac.uk) and A.J.C. (achadwick@caltech.edu).

References

Ainsworth, R. B., M. Salung, and S. T. C. Duivenvoorden (1999), Correlation technique, perforation strategies, and recovery factors—An integrated 3-D reservoir modeling study, Sirikit Field, Thailand, *AAPG Bull.*, *83*(10), 1535–1551.

Allen, J. R. L. (1965), A review of the origin and characteristics of recent alluvial sediments, *Sedimentology*, *5*, 89–191, doi:10.1111/j.1365-3091.1965.tb01561.x.

Allen, J. R. L. (1979), Studies in fluviatile sedimentation: An elementary geometrical model for the connectedness of avulsion-related channel sand bodies, *Sediment. Geol.*, *24*, 253–267.

Ashworth, P., J. Best, and M. Jones (2004), Relationship between sediment supply and avulsion frequency in braided rivers, *Geology*, *32*, 21–24, doi:10.1130/G19919.1.

Aslan, A., W. J. Autin, and M. D. Blum (2005), Causes of river avulsion: Insights from the late Holocene avulsion history of the Mississippi River, USA, *J. Sediment. Res.*, *75*, 650–664, doi:10.2110/jsr.2005.053.

Bianchi, T. S., and M. A. Allison (2009), Large-river delta-front estuaries as natural "recorders" of global environmental change, *Proc. Natl. Acad. Sci. U.S.A.*, *106*(20), 8085–8092.

Blum, M. D., and H. H. Roberts (2009), Drowning of the Mississippi delta due to insufficient sediment supply and global sea-level rise, *Nat. Geosci.*, *2*, 488–491.

Bohacs, K., and J. Suter (1997), Sequence stratigraphic distribution of coaly rocks: Fundamental controls and paralic examples, *AAPG Bull.*, *81*, 1612–1639.

Bresse, J. A. C. (1860), Cours de Mecanique Appliquee, Hydraulique.

Bridge, J. S., and S. D. Mackey (1993), A revised alluvial stratigraphy model, in *Alluvial Sedimentation*, edited by M. Marzo and C. Puigdefabregas, *Int. Assoc. Sedimentol. Spec. Publ.*, 17, pp. 319–336.

Brizga, S. O., and B. L. Finlayson (1990), Channel avulsion and river metamorphosis: The case of the Thomson River, Victoria, Australia, *Earth Surf. Processes Landforms*, *15*, 391–404.

Bryant, M., P. Falk, and C. Paola (1995), Experimental study of avulsion frequency and rate of deposition, *Geology*, *23*(4), 365–368.

Chamberlin, E. P., and E. A. Hajek (2015), Interpreting paleo-avulsion dynamics from multistory sand bodies, *J. Sediment. Res.*, *85*(2), 82–94.

Chatanantavet, P., and M. P. Lamb (2014), Sediment transport and topographic evolution of a coupled river and river plume system: An experimental and numerical study, *J. Geophys. Res. Earth Surf.*, *119*, 1263–1282, doi:10.1002/2013JF002810.

Chatanantavet, P., M. P. Lamb, and J. A. Nittrouer (2012), Backwater controls on avulsion location on deltas, *Geophys. Res. Lett.*, *39*, L01402, doi:10.1029/2011GL050197.

Chow, V. T. (1959), *Open-Channel Hydraulics*, 680 pp, McGraw-Hill, New York.

Coleman, J. M., and S. M. Gagliano (1964), Cyclic sedimentation in the Mississippi River deltaic plain, *Gulf Coast Assoc. Geol. Soc. Trans.*, *14*, 67–80.

DiBiase, R. A., A. B. Limaye, J. S. Scheingross, W. W. Fischer, and M. P. Lamb (2013), Deltaic deposits at Aeolis Dorsa: Sedimentary evidence for a large body of water in the northern plains of Mars, *J. Geophys. Res. Planets*, *118*, 1285–1302, doi:10.1002/jgre.20100.

Donat, M. G., A. L. Lowry, L. V. Alexander, P. A. O'Gorman, and N. Maher (2016), More extreme precipitation in the world's dry and wet regions, *Nat. Clim. Change*, doi:10.1038/nclimate2941.
Edmonds, D. A. (2012), Stability of backwater-influenced river bifurcations: A study of the Mississippi-Atchafalaya system, *Geophys. Res. Lett.*, *39*, L08402, doi:10.1029/2012GL051125.
Edmonds, D. A., D. C. J. D. Hoyal, B. A. Sheets, and R. L. Slingerland (2009), Predicting delta avulsions: Implications for coastal wetland restoration, *Geology*, *37*, 759–762.
Ganti, V., K. M. Straub, E. Foufoula-Georgiou, and C. Paola (2011), Space-time dynamics of depositional systems: Experimental evidence and theoretical modeling of heavy-tailed statistics, *J. Geophys. Res.*, *116*, F02011, doi:10.1029/2010JF001893.
Ganti, V., C. Paola, and E. Foufoula-Georgiou (2013), Kinematic controls on the geometry of the preserved cross sets, *J. Geophys. Res. Earth Surf.*, *118*, 1296–1307, doi:10.1002/jgrf.20094.
Ganti, V., Z. Chu, M. P. Lamb, J. A. Nittrouer, and G. Parker (2014), Testing morphodynamic controls on the location and frequency of river avulsions on fans versus deltas: Huanghe (Yellow River), China, *Geophys. Res. Lett.*, *41*, 7882–7890, doi:10.1002/2014GL061918.
Ganti, V., A. J. Chadwick, H. J. Hassenruck-Gudipati, B. M. Fuller, and M. P. Lamb (2016), Experimental river delta size set by multiple floods and backwater hydrodynamics, *Sci. Adv.*, *2*, e15101768.
Hajek, E., and M. A. Wolinsky (2012), Simplified process modeling of river avulsions and alluvial architecture: Connecting models and field data, *Sediment. Geol.*, *257–260*, 1–30.
Hajek, E., P. Heller, and E. Schur (2012), Field test of autogenic control on alluvial stratigraphy (Ferris Formation, Upper Cretaceous-Paleogene, Wyoming), *Geol. Soc. Am. Bull.*, *124*, 1898–1912.
Hamilton, P. B., K. Strom, and D. C. J. D. Hoyal (2013), Autogenic incision-backfilling cycles and lobe formation during the growth of alluvial fans with supercritical distributaries, *Sedimentology*, *60*, 1498–1525.
Heller, P. L., and C. Paola (1996), Downstream changes in alluvial architecture: An exploration of controls on channel-stacking patterns, *J. Sediment. Res.*, *66*(2), 297–306.
Hoitink, A. J. F., and D. A. Jay (2016), Tidal river dynamics: Implications for deltas, *Rev. Geophys.*, *54*, 240–272, doi:10.1002/2015RG000507.
Hooke, R. L. B. (1968), Model geology: Prototype and laboratory streams: Discussion, *GSA Bull.*, *79*, 391–394.
Hotchkiss, R. H., and G. Parker (1991), Shock fitting of aggradational profiles due to backwater, *ISH J. Hydraul. Eng.*, *117*(9), 1129–1144.
Hoyal, D. C. J. D., and B. A. Sheets (2009), Morphodynamic evolution of experimental cohesive deltas, *J. Geophys. Res.*, *114*, F02009, doi:10.1029/2007JF000882.
Hudson, P. F., and R. H. Kessel (2000), Channel migration and meander-bend curvature in the lower Mississippi River prior to major human modification, *Geology*, *28*, 531–534.
Jain, V., and R. Sinha (2003), Hyperavulsive-anabranching Baghmati river system, north Bihar plains, eastern India, *Z. Geomorphol.*, *47*(1), 101–116.
Jerolmack, D. J. (2009), Conceptual framework for assessing the response of delta channel networks to Holocene sea level rise, *Quat. Sci. Rev.*, *28*(17-18), 1786–1800, doi:10.1016/j.quascirev.2009.02.015.
Jerolmack, D. J., and D. Mohrig (2007), Conditions for branching in depositional rivers, *Geology*, *35*(5), 463–466.
Jerolmack, D. J., and C. Paola (2007), Complexity in a cellular model of river avulsion, *Geomorphology*, *91*(3-4), 259–270.
Jerolmack, D. J., and J. B. Swenson (2007), Scaling relationships and evolution of distributary networks on wave-influenced deltas, *Geophys. Res. Lett.*, *34*, L23402, doi:10.1029/2007GL031823.
Jones, L. S., and S. A. Schumm (1999), Causes of avulsion: An overview, in *Fluvial Sedimentology VI*, *Spec. Publ. of the Int. Assoc. of Sedimentol.*, edited by N. D. Smith and J. Rogers, pp. 171–178, Blackwell, Oxford, U. K.
Kim, W., D. Mohrig, R. Twilley, C. Paola, and G. Parker (2009), Is it feasible to build new land in the Mississippi River Delta?, *Eos Trans. AGU*, *90*(42), 373–374, doi:10.1029/2009EO420001.
Kleinhans, M. G. (2005), Flow discharge and sediment transport models for estimating a minimum timescale of hydrological activity and channel and delta formation on Mars, *J. Geophys. Res.*, *110*, E12003, doi:10.1029/2005JE002521.
Kleinhans, M. G., K. M. Cohen, J. Hoekstra, and J. M. Ijmker (2011), Evolution of a bifurcation in a meandering river with adjustable channel widths, Rhine delta apex, The Netherlands, *Earth Surf. Processes Landforms*, *36*, 2011–2027.
Lamb, M. P., J. A. Nittrouer, D. Mohrig, and J. Shaw (2012), Backwater and river-plume controls on scour upstream of river mouths: Implications for fluvio-deltaic morphodynamics, *J. Geophys. Res.*, *117*, F01002, doi:10.1029/2011JF002079.
Leonardi, N., A. S. Kolker, and S. Fagherazzi (2015), Interplay between river discharge and tides in a delta distributary, *Adv. Water Resour.*, *80*, 69–78.
Lynds, R. M., D. Mohrig, E. A. Hajek, and P. L. Heller (2014), Paleoslope reconstruction in sandy suspended-load-dominant rivers, *J. Sediment. Res.*, *84*, 825–836.
Mackey, S. D., and J. S. Bridge (1995), Three-dimensional model of alluvial stratigraphy: Theory and application, *J. Sediment. Res.*, *65*, 7–31.
Martin, J., B. Sheets, C. Paola, and D. Hoyal (2009), Influence of steady base-level rise on channel mobility, shoreline migration, and scaling properties of a cohesive experimental delta, *J. Geophys. Res.*, *114*, F03017, doi:10.1029/2008JF001142.
Meybeck, M., and C. J. Vörösmarty (2005), Fluvial filtering of land-to-ocean fluxes: From natural Holocene variations to Anthropocene, *C. R. Geosci.*, *337*(1), 107–123.
Miller, M. C., I. N. McCave, and P. D. Komar (1977), Threshold of sediment motion under unidirectional currents, *Sedimentology*, *41*, 883–903.
Mohrig, D., P. L. Heller, C. Paola, and W. J. Lyons (2000), Interpreting avulsion process from ancient alluvial sequences: Guadalope-Matarranya system (northern Spain) and Wasatch Formation (western Colorado), *Geol. Soc. Am. Bull.*, *112*(12), 1787–1803.
Mosley, M. P. (1975), Meander cutoffs on the River Bollin, Cheshire, in July 1973, *Rev. Geomorphol. Dyn.*, *24*, 21–31.
Nittrouer, J. A., J. Shaw, M. P. Lamb, and D. Mohrig (2012), Spatial and temporal trends for water-flow velocity and bed-material transport in the lower Mississippi River, *Geol. Soc. Am. Bull.*, *125*, 400–424, doi:10.1130/B30497.1.
Paola, C. (2000), Quantitative models for sedimentary basin filling, *Sedimentology*, *47*, 121–178.
Paola, C., and D. Mohrig (1996), Palaeohydraulics revisited: Palaeoslope estimation in coarse-grained braided rivers, *Basin Res.*, *8*, 243–254.
Paola, C., K. M. Straub, D. Mohrig, and L. Reinhardt (2009), The "unreasonable effectiveness" of stratigraphic and geomorphic experiments, *Earth Sci. Rev.*, *97*(1-4), 1–43.
Petter, A. L. (2010), Stratigraphic implications of the spatial and temporal variability in sediment transport in rivers, deltas and shelf margins, PhD thesis 205 pp., Univ. of Tex., Austin.
Powell, E., W. Kim, and T. Muto (2012), Varying discharge controls on timescales of autogenic storage and release processes in fluvio-deltaic environments: Tank experiments, *J. Geophys. Res.*, *117*, F02011, doi:10.1029/2011JF002097.
Reitz, M. D., and D. J. Jerolmack (2012), Experimental alluvial fan evolution: Channel dynamics, slope controls, and shoreline growth, *J. Geophys. Res.*, *117*, F02021, doi:10.1029/2011JF002261.

Reitz, M. D., D. J. Jerolmack, and J. B. Swenson (2010), Flooding and flow path selection on alluvial fans and deltas, *Geophys. Res. Lett.*, *37*, L06401, doi:10.1029/2009GL041985.

Rowland, J. C., K. Lepper, W. E. Dietrich, C. J. Wilson, and R. Sheldon (2005), Tie channel sedimentation rates, oxbow formation age and channel migration rate from optically stimulated luminescence (OSL) analysis of floodplain deposits, *Earth Surf. Processes Landforms*, *30*, 1161–1179.

Slingerland, R. L., and N. D. Smith (1998), Necessary conditions for a meandering-river avulsion, *Geology*, *26*, 435–438.

Slingerland, R. L., and N. D. Smith (2004), River avulsions and deposits, *Annu. Rev. Earth Planet. Sci.*, *32*, 257–285.

Stouthamer, E., and H. Berendsen (2001), Avulsion frequency, avulsion duration, and interavulsion period of Holocene channel belts in the Rhine-Meuse Delta, the Netherlands, *J. Sediment. Res.*, *71*, 589–598, doi:10.1306/112100710589.

Straub, K. M., V. Ganti, C. Paola, and E. Foufoula-Georgiou (2012), Prevalence of exponential bed thickness distributions in the stratigraphic record: Experiments and theory, *J. Geophys. Res.*, *117*, F02003, doi:10.1029/2011JF002034.

Swenson, J. B., V. Voller, C. Paola, G. Parker, and J. Marr (2000), Fluvio-deltaic sedimentation: A generalized Stefan problem, *Eur. J. Appl. Math.*, *11*, 433–452.

Syvitski, J. P. M., and Y. Saito (2007), Morphodynamics of deltas under the influence of humans, *Global Planet. Change*, *57*(3), 261–282.

Syvitski, J. P. M., et al. (2009), Sinking deltas due to human activities, *Nat. Geosci.*, *2*, 681–686.

Tessler, Z. D., C. J. Vörösmarty, M. Grossberg, I. Gladkova, H. Aizenman, J. P. M. Syvitski, and E. Foufoula-Georgiou (2015), Profiling risk and sustainability in coastal deltas of the world, *Science*, *349*(6248), 638–643, doi:10.1126/science.aab3574.

Törnqvist, T. E. (1994), Middle and late Holocene avulsion history of the River Rhine (Rhine-Meuse Delta, Netherlands), *Geology*, *22*, 711–714, doi:10.1130/0091-7613(1994)022<0711:MALHAH>2.3.CO;2.

Trampush, S. M., S. Huzurbazar, and B. A. McElroy (2014), Empirical assessment of theory for bankfull characteristics of alluvial channels, *Water Resour. Res.*, *50*, 9211–9220, doi:10.1002/2014WR015597.

van Dijk, M., G. Potsma, and M. G. Kleinhans (2009), Autocyclic behaviour of fan deltas: An analogue experimental study, *Sedimentology*, *56*, 1569–1589.

Vörösmarty, C. J., J. P. M. Syvitski, J. Day, A. de Sherbinin, L. Giosan, and C. Paola (2009), Battling to save the world's river deltas, *Bull. At. Sci.*, *65*(2), 31–43.

Williams, G. P. (1970), Flume width and water depth effects in sediment-transport experiments, *U. S. Geol. Surv. Prof. Pap.*, *562-H*, 1–37.